Technical University of Crete
Department of Electrical and Computer Engineering

Thesis

Automated Image Processing system for the analysis of small vessels of the microcirculation in the nailfold (Capillaroscopy)

Bantra Konstantina

Supervisor: Professor and Vice Rector Zervakis Michalis

Supervision committee: Professor and Vice Rector Zervakis Michalis
Professor Dollas Apostolos
Professor Pancaldi Fabrizio,
Department of Sciences and Methods for Engineering,
University of Modena and Reggio Emilia

June 26, 2020

Abstract

Over the years, nail-fold capillaroscopy has emerged as a safe, non-invasive, and accurate technique that can be used in determining the characteristics and the morphology of the blood capillaries near the nail-fold area. Various scholars have proved the connection between the morphology of the blood capillaries and the risks of rheumatic diseases such as the System Sclerosis. While nail-fold capillaroscopy has been in practice since the early 1970s, assessment of blood capillaries is still mainly performed using visual examination by medical officers. Thus, the objective of this study is to design an automated image processing system which will ease the diagnostic process by providing the doctors with more information on the state of the capillaries. This way the system will, in the long run, help in reducing diagnostic ambiguity and also in creating more concise and realizable results. For this thesis, the processing system was developed using the Matlab environment due to its ability to automate the entire imaging process, its ability to distinguish the characteristics, and the consequent evaluation of the associated features of the capillaries such as the capillary length and width.

Acknowledgments

As without his guidance this thesis would not have never been possible, I would like to express the deepest appreciation to my supervisor, Professor and Vice Rector Zervakis Michalis for his constant guidance, patience and support.

I would also like to thank my committee members, Professor Dollas Apostolos and Professor Pancaldi Fabrizio, who offered their insightful comments and advises on the thesis and I would like to offer my special thanks to Professor Pancaldi Fabrizio for kindly providing the dataset, without which this project would not have been realized.

Furthermore, I am particularly grateful for the assistance given by the Display Lab Supervisor Konstantia Moirogiorgou for her mentoring, encouragement and early insights that helped launch a big part of this thesis.

Finally I would like to thank my family and my friends for their continuous love and support that has been shown to me during my college years.

I will forever be grateful.

Contents

List of Figures

Chapter 1

Introduction

1.1 Motivation and Objectives

Over the past few decades there has been a significant increase in the frequency of autoimmune diseases [8]. Unfortunately, these diseases are extremely difficult to diagnose due to the overlapping of the symptoms with other diseases as well as the fact that they can affect different parts of the body. According to a survey conducted by the American Autoimmune Related Diseases Association (AARDA), it can take up to 4.6 years and 5 different physician visits before a patient receives a proper autoimmune disease diagnosis [9]. However, in the case of a disease, early diagnosis and treatment can play a critical role in the success of a treatment and offer more chances of longer survival. This highlights the need for more specialised diagnostic techniques that can aid the doctors during a diagnostic procedure by providing more data and thus more insight into a patient's health condition.

One of the most promising techniques for this purpose is nailfold capillaroscopy. The capillaroscopic technique is aptly named; it is the imaging of the capillaries located in the nail-fold bed. Some of the main advantages of this method are the fact that it is portable, simple to use and of low cost. Most importantly though, it has the potential to offer highly accurate results in rheumatic autoimmune diseases as it enables the imaging of micro-vascular structures of the skin and of the microcirculation. Nowadays, capillaroscopy is most used by physicians in order to evaluate patients suffering from Systemic Sclerosis

(SSc) or the Raynaud's phenomenon. As SSc has high morbidity and mortality rates, a lot of research has been dedicated to improving the methods and techniques that allow early detection, including nail-fold capillaroscopy.

The evaluation of the capillaroscopic images is one of the most important steps in the diagnostic procedure. Heretofore, the process of assessing the images was predominantly based on the visual observation of well-trained doctors. As a result, it has been very difficult to establish standardisation in the measured parameters. This has led to the use of different qualitative and semi-qualitative methods in various capillaroscopic studies. But as these methods are very difficult to interpret correctly and to compare against other cases there has also been a limited use of quantitative methods. However, the rapid advancement of technology in recent years has enabled the digitisation of the images acquired during the capillaroscopy examination. Furthermore, these images are of higher definition and thus, it is possible to process them digitally using cutting edge software tools that can extract more information and data from the images in a very short amount of time.

The topic of this thesis is the digital processing of images obtained by the nailfold capillaroscopy technique in order to accurately measure the structural features of the capillaries and to analyse as well as quantify, capillary abnormalities. This way, a doctor will have more quantitative measurements at their disposal to rely on, in order to evaluate a patient's state of health. In addition, the time required by the doctor to determine a diagnosis will be significantly reduced.

1.2 The Nail-fold Capillaroscopic Technique

Nailfold capillaroscopy is a diagnostic imaging technique for the capillaries and the microcirculation of an individual and it can be applied on numerous areas on a person's the skin. The most frequent places chosen for this imaging technique are the patient's limbs and, in particular, the nailfold area. The reason behind this is that the access to those areas is much easier compared to the ones of the retina and the inside of the lip. In addition to that, the area of the nail-fold is well

defined as opposed to the other ones. Furthermore, the extent of the distortion of the capillaries located in the nail-fold area can not only indicate the severity of the disease in the microcirculation of a patient, but also its progression on vital organs. Additionally, there have been many recent studies indicating that further analysis of the capillaries' characteristics located in the nailfold could lead to the early prognosis of cardiovascular problems [10].

Nailfold capillaroscopy was first introduced more than 400 years ago when Johan Christophorous Kolhaus used a primitive form of a microscope in order to observe the capillaries located in the nail-fold. After that, a number of renowned scientists and physicians started working on proving an association between the structure of the capillaries and the existence of an underlying disease. Physiologist Johann Evangelist Purkinje, physician Giovanni Rasori and surgeon Carl Hueter are only a few of the scientists that laid the foundations for the study of microcirculation. However, it was in 1973 with the groundbreaking work of Hildegard Maricq and Carwile LeRoy, that nail-fold capillaroscopy was put on the spotlight and piqued the interest of the research community. These two scientists were the first to describe and publish two typical capillaroscopic patterns for SSc, the slow pattern and the active pattern. Thirty years after their publication, capillaroscopy is now officially considered both an essential and a mandatory diagnostic tool for the classification of SSc by the European League Against Rheumatism (EULAR) and the American College of Rheumatology (ACR) guidelines.

1.2.1 Capillaroscopy Devices
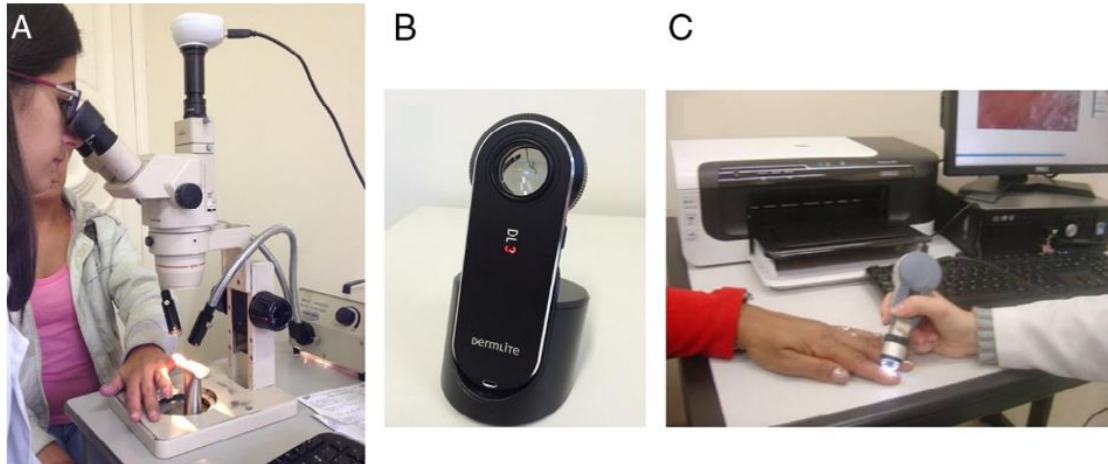
Figure 1.1: Devices that can be used for the nailfold capillaroscopy examination: (A)Stereo-microscope (B)Dermatoscope (C) Videocapillarosope [1]

In general, there are three main device categories that can be used to obtain an image of the capillaries:

- *Stereo-microscope:* This particular device is the one most frequently used, because it is easy to use. Its main disadvantage is that it has low magnification capacity that ranges between 10 and 50 times and, as a result, the obtained images have low quality.

- *Ophthalmoscope and Dermatoscope:* The use of these devices was originally not intended for the capillaroscopy examination, however they can be used in the absence of a better alternative. These two devices have low magnification capacity that ranges between 10 and 20 times and therefore the obtained images have low quality.

- *Videocapillaroscope:* This particular device was designed exclusively for the examination of capillaroscopy and therefore is equipped with several different lenses with high magnification capacity that ranges between 100 and 600 times as well as a digital camera. This way the obtained images are of high quality which we can process digitally using special software tools.

1.2.2 Examination procedure

When a patient visits a doctor's office in order to have the capillaro-
scopic examination, the first thing they have to do is relax and remain
in a calm state for approximately 20 minutes before the imaging in
order for their capillaries to return to their normal state. Otherwise
the results of the capillaroscopy may contain inaccuracies. This is
because of the role that the skin plays in the thermoregulation of the
human body which can lead to vasodilation or vasoconstriction of the
capillaries. After the 20 minutes have passed, the patient enters the
examination room, sits on a chair and rests their hands on a table at
chest height. In order to complete the capillaroscopic technique, the
nailfold microvascular bed of the 2nd, the 3rd, the 4th and the 5th
nail of each hand will be examined. The only exception is when a nail
presents an active infection or a wound. Usually the 4th and the 5th
fingers offer better imaging as their subpapillary venous plexus has
better visibility.

At the start of the examination, a drop of immersion oil is placed on
the patient's nails to improve the quality of the image by creating a
smooth surface on top of the nail. Afterwards, the Videocapillaro-
scope is placed sequentially above each nail and an image is obtained.
During this procedure the doctor has to be careful not to apply any
pressure on the fingers as it could interfere with the results. To com-
plete the capillaroscopic examination, 4 photos are obtained for each
nail, 32 images in total for every patient. Subsequently, the doctor has
to evaluate each image separately in order to make a correct diagno-
sis.

1.2.3 Image evaluation process

To this day, in order for a doctor to evaluate a capillaroscopic image,
a series of measurements have to be obtained based on the visual ob-
servation of the image and, usually, with the assistance of a software
tool. Firstly, the doctor will count the number of capillaries that lay
within a 1mm length of the distal row of each finger. Usually, the way
that capillaries are counted is by placing the cursor over the capillary
and selecting it. Then, the size of each capillary is measured in search

for giant capillaries that usually indicate the existence of an underlying disease. The distance between two points of interest can also be measured by a doctor by selecting them with his cursor. Finally, the doctor will examine the image for microhaemorrhages or twisted capillaries. Based on the results of all the aforementioned examinations, the doctor can decide on the state of health of a patient and provide a correct diagnosis.

1.2.4   Application Requirements

The quality of the images obtained during the capillaroscopic procedure plays a critical role in the performance of the suggested method. In order for the algorithm to work, the images must contain as little as possible reflective areas and air bubbles which are usually caused by the vegetable oil placed on the patient's fingers. Furthermore, the higher the magnification factor used during the imaging, the better the results tend to be. That is because thin objects are very challenging to detect, so by using higher magnification the vessels appear thicker in the image. Finally, it is important to note that the presence of microbleedings might interfere with the final results as they tend to be identified as capillaries since their shape and size is very similar to that of the capillaries.

1.3   Thesis innovation

As the medical imaging field embraces new applications of computer science, digital image processing can produce innovative analysis methods which can have a huge impact on the medical field. The present thesis aims to contribute in the further development of the field by adding a fully automated system which will process images obtained from the capillaroscopic technique, to the evergrowing list of computer applications in the medical field. In particular, one of the innovations of the thesis is the presentation of a new pre-processing approach for the capillaroscopic images. However, the most important aspect of the thesis is that each image is evaluated in a two level approach. That is, a feature vector is extracted from the image as a whole as well

as for each capillary individually. This gives us the opportunity to calculate new features and extract more information for every image processed.

1.4   Outline of thesis

The present thesis is divided in 7 chapters. Chapter 1 of the thesis is a brief introduction to the basic background information about NC techniques. Chapter 2 provides the necessary biological background regarding the anatomy and physiology of the normal capillaries as well as the expected deviations associated with some of the most common rheumatological diseases. Chapter 3 presents the literature review on current research conducted on extracting capillary characteristics from capillaroscopic images. Chapter 4 provides a technical background of the methods used in our proposal. In Chapter 5 we present an algorithmic pipeline for the evaluation of capillaroscopy images. In Chapter 6 are described some application examples and their final results. Lastly, Chapter 7 includes our conclusions and discussion alongside with a proposal for future work.

Chapter 2

Biological Background

2.1 Physiology of capillaries

Nailfold capillaroscopy, as the name implies, is an imaging technique for the capillaries located in the nail-fold area. Capillaries, are the smallest blood vessels of the body. They are only one cell thick, thus allowing only one red blood cell to pass at a time [11]. The capillaries of a human, form a dense and complex network of "loops" (U-shaped structures commonly compared to hairpins), with an afferent (arterial) and a draining (venous) limb connected by an apex (an apical loop). The capillaries play a vital role in the diffusion of gasses and the movement of substrates and non-essential by-products of cellular respiration. The density of the capillaries is an especially important parameter as it determines the total surface area available for exchange across capillaries as well as the maximum distance between a cell and blood, and thus diffusion time. The capillary density and length are two particularly crucial factors that contribute significantly to the total resistance of the capillary bed which affects the blood flow inside the body. Variations in capillary blood flow or pressure may influence the transcapillary exchange processes, the results of which could vary depending on the extent of the disruption. Capillaries are also a key factor in preserving tissue fluid homeostasis. This is very important as homeostasis ensures the proper function of the cells of the body, as it provides them with all the necessary materials such as glucose and oxygen. Homeostasis is regulated by the four Starling's

forces: hydrostatic pressure in the capillary, hydrostatic pressure in the interstitium, oncotic pressure in the capillary and oncotic pressure in the interstitium. Out of the four, the hydrostatic pressure is the most variable one. Slight changes in the capillary pressure can lead to major effects in the transcapillary fluid exchange and thus in homeostasis [12].

Most of the skin blood vessels originate from deeper lying muscles and subcutaneous fat and go straight through the fascia into the dermis. In the dermis, there are two major categories of vessels: the ones lying deeper in the hypodermis- which form the quarter plexus- and the more superficial ones that connect with the subpapillary plexus and are located 1–2 mm below the surface of the skin. The superficial vessels are a lot thinner, usually their size ranges from 10 to 35 um, compared to the ones laying in the hypodermis, whose size ranges 40–50 um. Each vessel in the quarter plexus, branches off into an arteriole which supplies blood to the subpapillary plexus and from these arise the capillary loops of the dermal papillae. The capillaries then drain into a venule which connects with the original blood vessel.

Unfortunately, the access to the vascular bed is difficult, making the examination of the capillaries extremely limited. Additionally there are very few techniques available that can be used for this type of examination. One of the reasons is the fact that there was a misconception about the ability to calculate the blood flow pressure as well as the mechanisms of the capillaries by extrapolating data from larger vessels of the body. However, after a lot of research tested on animals, this theory was refuted. Thus, there is no alternative but to investigate the capillary structure and functionality directly on the capillaries. Most of the research has been carried out on capillaries of the retina, lip and skin with the vast majority focusing on capillaries located in the nail-fold as the access to these areas is relatively easier.

2.1.1 Aging and site effects on the capillaric anatomy

Histological studies performed on human epidermis have shown that the anatomy of the blood vessels and in particular, the anatomy of the capillaries varies on different areas of the body. In most areas of the

body, the loops are perpendicular to the skin surface, so only the top, which connects the two limbs, is visible and has a crescent shape. The main advantage of the capillaries located in the toe and finger nailfold is that the capillary loops lie parallel to the surface of the skin, which allows imaging along their entire length. For the sake of accuracy, we are not able to visualise the capillaries themselves, as their thin walls are essentially transparent, but instead we visualise the column of red blood cells that moves inside them.
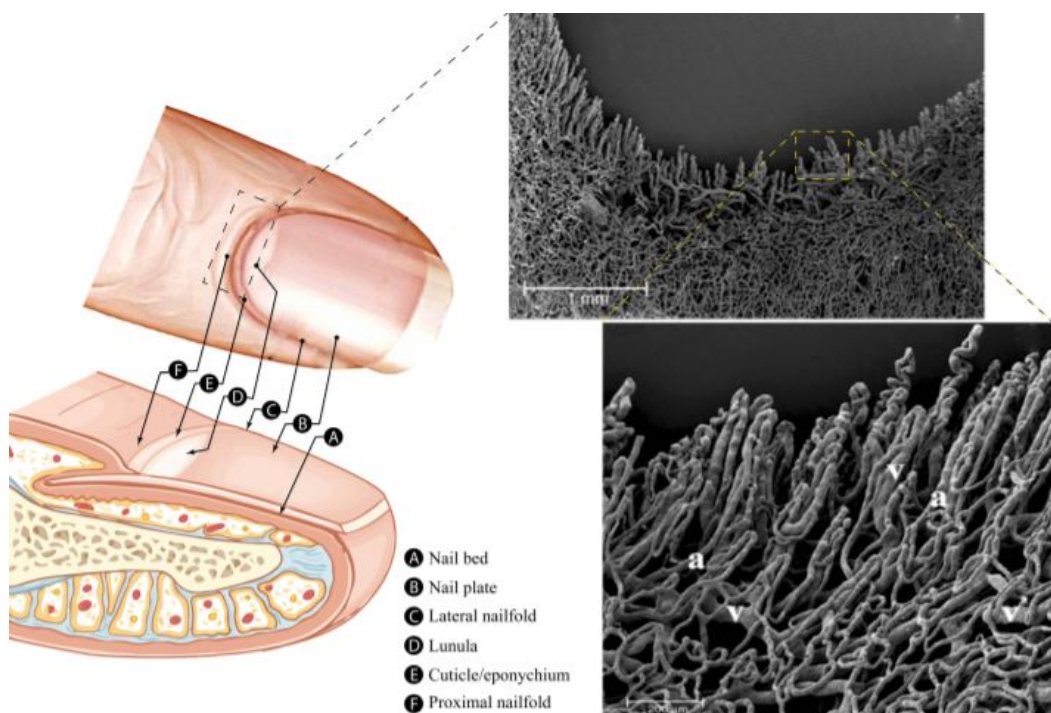
Figure 2.1: Illustration of nailfold anatomy. [2] [3]

The capillaric density also varies in different areas of skin. Additionally, the density is also affected by the patient's age. That is because angiogenesis, the body's ability to create new microvascular structures, is severely impaired by ageing. As a result, as a person ages, their capillaric density decreases. Aging can also affect the capillaric length and can cause disorganisation of the nailfold bed geometry. Finally, another important parameter that we should take into consideration when performing the capillaroscopic examination is the visibility of the subpapillary venous plexus. Usually the visibility is better on children and Caucasian people.

2.2 Measuring capillaric structural characteristics

After extensive research on capillaric structure, clinicians were able to associate changes in structural elements with underlying connective tissue diseases. So, when evaluating a capillaroscopic image, some of the features of interest are the following: the capillaric density, width, capillaric length, arterial limb diameter, venous limb diameter, its width variations as well as the capillary distribution which is affected by the capillaric orientation [4].

The height and width of the capillaries can be used as primitive indicators of the health condition of an individual. For example, a person with elongated capillaries usually suffers from hypertension and arteriosclerosis. On the contrary, the presence of shorter capillaries in the capillaroscopic images of a person often points to cardiac insufficiency. Some of the structural elements of interest are annotated in the schematic drawing of the front part of a nailfold capillary loop bellow.
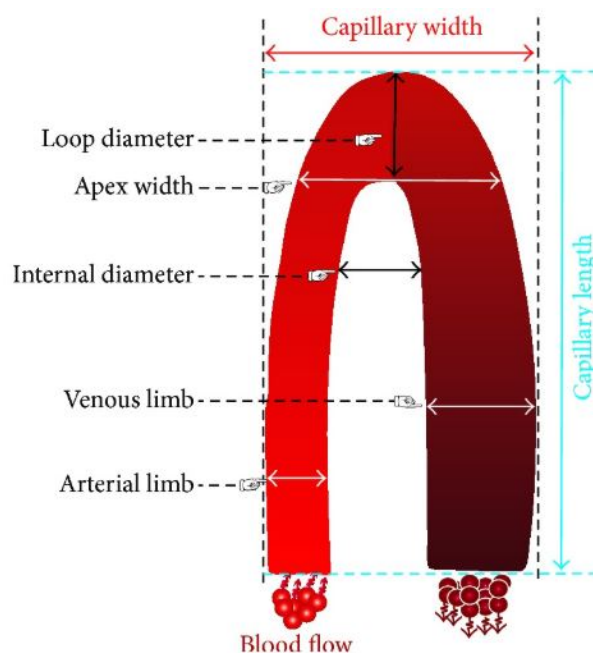
Figure 2.2: Schematic drawing of the front part of a nailfold capillary [4].

Capillary Width

In order to measure any capillaric feature, first it has to be strictly defined. Unfortunately, the capillary width has been a very controversial parameter, as there is no general consensus towards its definition, therefore causing a lot of disagreement on the topic. However, most of the researches are in favour of the definition of the width of the capillary as the width of the loop at its widest section. Some other names that came up in the literature that also describe capillary width are: "loop width", "maximum loop width", "total width","total calibre of loop","capillary loop amplitude","total capillary width" and "external diameter".

Because of this difference of opinion amongst scientists it has also been also very difficult to set the limits in which a capillary's width is considered normal as well as when it should be considered deformed. Based on the definition mentioned above, in adults, the upper limit for a capillary to be considered healthy ranges from 25 to 50 um. Additionally, most of the researchers choose Maricq's work [13] as their reference point, which defines capillary enlargement as a 4- to 10-fold increase of the capillary size.
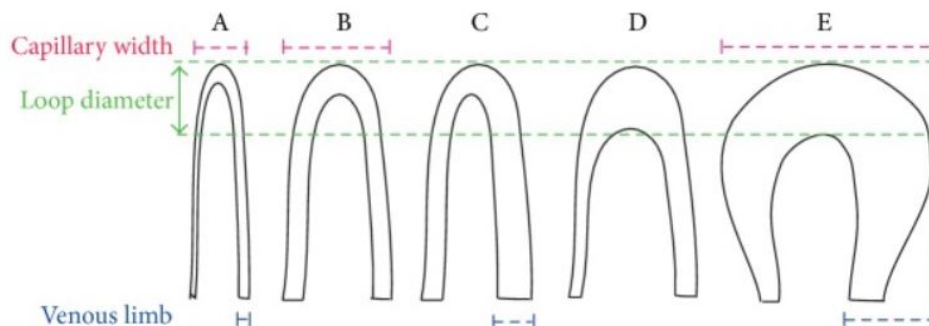
Figure 2.3: Enlarged Capillary Loops: A)normal capillary loop B) enlarged capillary loop C) enlarged efferent capillary loop D) enlarged apical capillary loop and E) giant capillary loop [4]

Capillary Length

We define length of the capillary as the distance between the apex of a capillary loop to the point where the limbs of the capillary loop are

no longer visible. Some other commonly used terms in the bibliography used to describe capillary length are: "loop length" and "capillary height". For a healthy person, the capillaries of their identical fingers in their right and left hand have usually very similar lengths, with the exception of an injured finger or one with an active infection. The capillaries whose length is up to 300 um are considered healthy while those whose length is more than 300 um are described as elongated. A prime example of the importance of capillaric length is the fact that in the capillaroscopic images from patients suffering from diabetes, the capillaries are usually shorter, sometimes up to only 10 um long.

Capillary Density

The density of the capillaries has been strongly associated with the existence of an underlying connective tissue disease, thus making it one of the most important features that must be calculated in a capillaroscopic image. The bibliography defines capillaric density as the number of capillaries in a 1 mm length of the distal row of each finger or toe. Often, capillaric density is also referred to as the "number of capillaries" and "capillaries number". Usually a healthy adult has a capillaric density ranging from 7.3 to 10.3, while children have a lower capillary density, ranging from 5 to 7.3.

Capillary Limbs Width

The two limbs of a capillary have different roles in the microcirculation, and so their structures have some important differences. The arterial limb, or afferent branch, is responsible for transporting blood rich in oxygen to the epidermal cells. On the other hand, the efferent branch, or the venous limb, is responsible for transporting blood low in oxygen and high in waste products back to the heart for reoxygenation. Similarly to the capillary, the arterial limb width and venous limb width are defined as the diameter of the arterial and venous limbs at their widest sections. Other commonly used terms to describe the arterial and venous limb width are: "afferent limb width" and "efferent limb width" respectively. The capillary of a healthy individual has a less wide arterial limb than a venous one. The venous limb can even be

up to 1.5 times as wide as the arterial limb. For a healthy individual, the arterial width ranges between 7 and 17 um while the venous width ranges from 11-20 um.

Capillary Distribution

Normally, when examining the capillaroscopic images of a healthy individual it is obvious that the capillaries are distributed homogeneously throughout the nailfold bed. They also lie parallel and very close to each other in order to supply blood to every single epidermal cell. This capillaroscopic pattern is referred to as regular capillary distribution and it is also observed in children. Should the capillaries not lie in parallel or overlap with each other, then this capillaroscopic pattern is referred to as capillary disorganisation or disorganised architecture.

Capillary Orientation

In order to better define capillary disorganisation we use two parameters to describe every capillary: capillary direction and capillary polarity. We define capillary direction as the angle between a vertical line and the vector associated with the highest proper value. Respectively, we define capillary polarity as the standard deviation from a main direction of all the capillary directions in an image.

2.3 Capillaroscopic patterns

2.3.1 Normal capillaroscopic pattern

For a healthy person a typical capillaroscopic image has the following characteristics: similar capillaries in regard to size, shape and colour. Furthermore, the capillaries lie parallel to each other and transversely across the nailfold bed. However, it is quite common for the capillaries to have morphological variations, for example to be twisted or overlap with another capillary. Additionally we expect to have a normal capillary density, which is obtained by counting the number of loops in one millimetre. Usually normal capillary density ranges from 7 to 12

capillaries, averaging 9 $\frac{capillaries}{mm}$ [5]. As fingers are very susceptible to
trauma, it is completely normal to notice presence of a small num-
ber of capillary dilations and areas of devascularisation. Furthermore,
we can also expect to find areas with micro-bleeding if the trauma is
recent. In general, when examining a capillaroscopic image, it is espe-
cially important to remember that there is great variation in the shape
and size of the capillary loops of healthy people, and even among the
fingers of the same person.
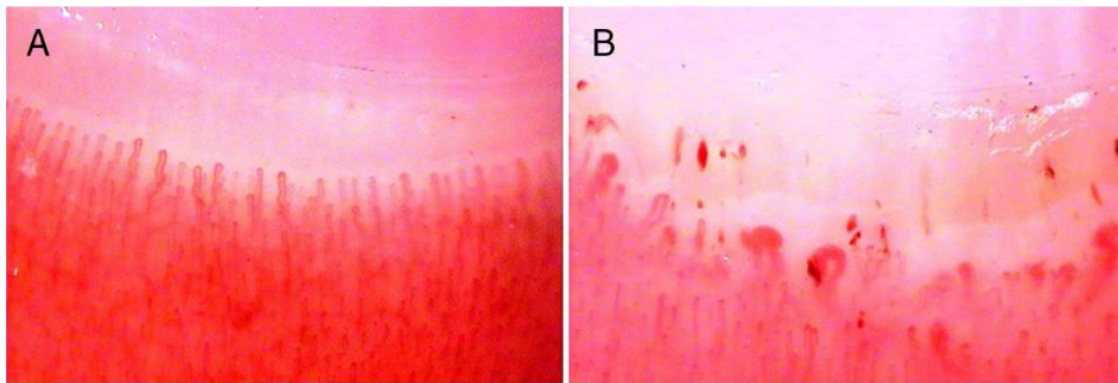
Figure 2.4: Images of capillaroscopy with a normal capillaroscopic pattern (A) and
with SD pattern (B) [5]

Scleroderma pattern

The Scleroderma pattern was first described by Maricq et al. [13] in
1981 and it was revised in 2004. The typical pattern observed in cap-
illaroscopic images includes the presence of dilated or giant capillaries,
a reduced number of capillary loops and avascular areas, microhaem-
orrhages and neoangiogenesis.

After its revision, the scleroderma pattern was divided into three sub-
divisions: the "early" pattern, the "active" pattern and the "late" pat-
tern. The "early" pattern is characterised by micro-haemorrhages and
dilated capillaries while the capillary homogeneous distribution is still
preserved. In the "active" pattern there is a presence of giant capillaries
and micro-bleedings as well as a distortion of the capillary architec-
ture. Finally, in the "late" pattern, there are very few giant capillaries
as there is severe loss of capillaries. The presence of neoangiogenesis
is visible as well as large avascular areas.

The Scleroderma pattern is found in 80-90% of patients suffering from Systemic Sclerosis but it can also be found in other autoimmune rheumatic diseases or in mixed connective tissue diseases. The identification of the existence of the "early" scleroderma pattern is crucial for the early diagnosis of systemic sclerosis.

2.3.2 Capillaroscopic patterns of autoimmune rheumatic diseases

Systemic Sclerosis

Systemic sclerosis is an autoimmune disorder that usually involves the damaging of internal vital organs e.g. the lungs, the heart and the kidneys. Due to the severance of the disease, the morbidity and mortality rates are very high. On that account, a lot of research has been dedicated to finding a way for an early diagnosis and early treatment, when there has yet to be severe damage to the internal organs that can't be reversed. It is at this stage that nailfold capillaroscopy could play a critical role. Since 2013, the importance of nailfold capillaroscopy in identifying patients with Systemic Sclerosis has only increased. This is also highlighted by the fact that very recently the Research Group on Scleroderma from EULAR (European League Against Rheumatism) suggested the consideration of the three subdivisions of the Scleroderma pattern combined with the presence of swollen fingers and a positive result for antinuclear factor as preliminary criteria in order to diagnose SSc.

As it has already been mentioned, the Scleroderma pattern is visible in the nailfold capillaroscopic images of approximately 90% of patients suffering from Systemic Sclerosis. The typical micro-angiopathy in SSc cases that is observed includes dilated or giant loops, decrease of capillaric density, the presence of avascular areas, micro-bleedings, neoangiogenesis and disruption of the capillaric architecture. These distortions are typically observed in the early stages of the disease, when the clinical suggestion points towards the Raynaud's Phenomenon. Unfortunately, there has yet to be a proven correlation between the distortions in the capillary architecture and the duration of the disease.

There are a lot of researchers who support the presence of dilated capillaries and micro-haemorrhages suggests a few years of disease, while a more intense disorganisation and devascularisation suggest a disease in its later stages. However, it is not uncommon to find patients with many years of illness and little devascularisation or patients with little years of illness and severe capillaric disorganisation.

Systemic Lupus Erythematous

Changes in the capillaric structure in the capillaroscopic images are unfortunately vaguer in the case of Systemic Lupus Erythematous (SLE) than that of Systemic Sclerosis where in the later case the Scleroderma pattern is present. Some common abnormalities observed in the capillaroscopic images of patients suffering from SLE are elongated, meandering or even completely twisted capillaries. Additionally, there are areas where capillary loss is evident and generally the subpapillary plexus is more visible. These characteristic changes only appear to approximately 50% of the patients. Meanwhile, these abnormalities are more prominent in patients suffering from both Systemic Lupus Erythematous and the Raynaud's Phenomenon.
The role of nailfold capillaroscopy in SLE patients was, once more, highlighted in a recent research focused on the detection of pulmonary arterial hypertension. The results of this research suggested that patients suffering from SLE should have nailfold capillaroscopy once a year in order to diagnose the existence of pulmonary arterial hypertension early [14].

Dermatomyositis and Polymyositis

Patients suffering from Dermatomyositis present the typical Scleroderma pattern more frequently than patients with Polymyositis, when having the capillaroscopic examination. However, in both cases, the rates are low, ranging from 10 to 60%. Typical capillaroscopic findings of these diseases include reduced capillary density, dilated capillaries and disruption of the capillary architecture. In this case, the structural changes of the capillaries have been associated with the severity of the diseases as well as interstitial pulmonary involvement [15].

Mixed Connective Tissue Disease

Usual capillaroscopic findings for patients suffering from Mixed Connective Tissue Disease (MCTD) include micro-bleedings and disorganisation of the capillaries. Unlike in the case of Systemic Sclerosis, the presence of giant capillaries or capillary density reduction is rare. As the Raynaud's Phenomenon is very commonly one of the initial symptoms of MCTD, for about 85% of patients, it is also used as a classification criterion for the diagnosis of the disease [16].

Primary Sjögren Syndrome

The Scleroderma pattern is usually present in only 13-30% of the patients suffering from Primary Sjögren Syndrome. This percentage highly depends on whether or not there is presence or absence of Raynaud's Phenomenon. Unfortunately, in case of the absence of the Raynaud's Phenomenon, the capillaroscopic results of more than 50% of the patients appear to be normal. On the contrary, when the Raynaud's Phenomenon is present, the capillaroscopic results might be vague, but, they usually include tortuous or irregularly shaped capillaries as well as increased visibility of the subpapillary plexus. Finally, the presence of the typical scleroderma pattern in patients suffering from Sjögren Syndrome is very rare [17].

Rheumatoid Arthritis

In the case of Rheumatoid Arthritis there hasn't been extensive research on the correlation between capillaroscopic imaging and the existence of the disease. However, there have been a few reports suggesting the presence of increased capillaric length, tortuous capillaries and increased visibility of the subpapillary plexus. Nevertheless, the presence of the Scleroderma pattern in in patients with Rheumatoid Arthritis has yet to be proven [18].

Antiphospholipid Syndrome

The most particular capillaroscopic finding in patients suffering from Antiphospholipid Syndrome is the presence of symmetrically distributed

micro-bleedings on their nailfold bed. These results, in conjunction with clinical tests proving the existence of IgG and IgM anticardiolipin antibodies, suggest a direct damage to the vascular endothelium [19].

Chapter 3

Bibliography

In this chapter we introduce the bibliographic research we conducted in order to gain knowledge on the topic of the segmentation of images of vascular structures and based on which we would begin our own approach. We also include a short summary of the theoretical background of each studied method as well as some of the main advantages and disadvantages of them. The research started off more generally on segmentation methods, which is a very large research field in image processing. It is used for medical imaging of biological structures such as neurons, vessels or even cells. These applications highly resemble the images obtained during the capillaroscopy examination as they present the same challenges when digitally processed. Firstly, the objects of such images have very similar features that need to be enhanced while the noise must be reduced in order to improve the quality of the image. Secondly, in most applications, the images have to be segmented and classified for automatic feature extraction. However, the biggest challenge those applications provide is that of reliability. It is crucial for medical applications to present a low rate of false positive results and an even lower rate of false negatives. For this reason all the algorithms used for medical application undergo severe evaluation processes before they can be used in practise.

3.1 Techniques used for nailfold capillaroscopy images

3.1.1 Image pre-processing

The work of N. P. Doshi, Schaefer, G., and A. Merla, *"An evaluation of image enhancement techniques for capillary imaging"* [20], was very useful for this part of the bibliographical research. The authors of the paper assembled ten different enhancing filtering techniques suggested by other researchers and compared their results in order to find which of them preserved the edges of the capillaries best. The researchers selected two images for every nailfold capillaroscopic class and after applying all the selected filters, they applied a Sobel edge detecting filter and compared the results.

The filters the authors chose to compare to one another were: the median filter, the Gaussian filter, the a-trimmed filter, the Band-pass ϵ filter, the anisotropic diffusion filter, the bilateral filter, the Bilateral Enchancer, the Wavelet filter, the Non Local Means (NLM) filter and finally the Adaptive Damped Wave Equation (ADWE). According to the results, the filters could be ranked in an accenting order as a-trimmed filter, Wavelet filter, Band-pass ϵ filter, Gaussian filter, ADWE filter, median filter, anisotropic diffusion filter, NLM filter, bilateral filter and bilateral enhancer, with the a-trimmed filter having the worst performance at 0.1629 and the bilateral enhancer the best at 0.3872. Another interesting result of the study is the fact that when the results of the filtering techniques are compared to the results obtained from the original images *e.g. without any processing) the filters a-trimmed, Wavelet, Band-pass ϵ and Gaussian actually perform worse than the original image. However, it is important to note that the results described are based on only one edge detection algorithm so they can be misleading.

Since the publishing of the paper mentioned above in 2006 there have been many other suggested filtering approaches for capillaroscopic images, as the interest in nailfold capillaroscopy is only rising. Another promising approach is that of Gabor Hamar, G. Horvath, Zs. Tarjan

and T. Virag titled *"Markov Chain Based Edge Detection Algorithm for Evaluation of Capillary Microscopic Images"* [21]. The authors identified a problem on the previously suggested methods, it being the fact that the researchers performed intrapixel processing on the image, so they suggested a method that took into consideration the interpixel relations using the Markov Chain. Some of the biggest challenges the researchers had to overcome when processing the capillaroscopic images were the extensive blur, the noise and the low contrast of the images. However, these problems are caused by the very basis of the imaging technique which is that the capillaries are observed through the skin, so they must be handled using digital processing.

In brief, the approach the researchers suggested is based on the calculation of the second derivative of every pixel (x,y) in order to identify the centerline of the capillaries, as follows:

$$
A|_{x_0,y_0} = \begin{bmatrix} \dfrac{\partial^2}{\partial x^2} f|_{x_0,y_0} & \dfrac{\partial^2}{\partial x \partial y} f|_{x_0,y_0} \\ \dfrac{\partial^2}{\partial x \partial y} f|_{x_0,y_0} & \dfrac{\partial^2}{\partial y^2} f|_{x_0,y_0} \end{bmatrix}
$$

Then, using the following "walking" algorithm they process the whole image.

---

a Walking Algorithm(f) [21]

1: s←START_POINT()
2: v_0 ←0
3: w←(s)
4: **while** !STOP_CONDITION() **do**
5:     s_1 ←NEXT_POINT(f, s, v_0)
6:     $v_0 \leftarrow s_1 - s$
7:     $s \leftarrow s_0$
8:     $w \leftarrow s$ appended to w
9: **end while**
10: **return** w

---

b NEXT_POINT(f, x, y, v_0) [21]

1: Calculating A in point (x,y)
2: v←the normalized eigenvector of A belonging to the smaller eigenvalue
3: **if** $v_0^\top v < 0$ **then**
4:     v ← -v
5: **end if**
6: v_0 ←v
7: p← $(x, y)^\top + v \dot{c} onst$
8: l←section through p, which is perpendicular to v
9: q←minimum point of $f(x, y)$ from the points of l **return** q

One of the main advantages of the proposed method is that the results are very precise, with a 91% vessel detection, which is better when compared to other edge detection filters. It is important to note that the results the researchers provided were based on the opinion of a human observer. One of the main disadvantages of this proposal is that it requires up to 100 iterations in order to provide good results. Generally, the more the iterations, the less the noise present in the resulting image. However, as the iterations increase, the edges of the capillaries can become disconnected or even disappear. Additionally, the time required for the processing to finish is too long due to the high number of iterations.

The researchers Niraj P. Doshi, Gerald Schaefer and Shao Ying Zhu proposed a method of improvement of the binarisation and the skeleton extraction of the nailfold capillaroscopy images by focusing on reducing the non-uniform background. After studying the work of Wen et al. and Lo et al. who used histogram equalization and the isolation of the green channel respectively, they decided that their results were inadequate as their approaches were too simple. Thus, they decided to filter the images using a Difference of Gaussian (DoG) filter in order to make the background of the images uniform while preserving the capillary edges. The DoG filter is defined as:

$$h(x,y) = \frac{1}{2\pi}[\frac{1}{\sigma_1^2}exp(-\frac{x^2+y^2}{\sigma_1^2}) - \frac{1}{\sigma_2^2}exp(-\frac{x^2+y^2}{\sigma_2^2})] \qquad , where \quad \sigma_1 < \sigma_2$$

The researchers set the value of σ_2 as the average capillary width and $\sigma_1 = \frac{\sigma_2}{1.6}$. After testing several thresholding techniques, they selected Otsu's method as the best in order to binarise the image and lastly applied a series of post-processing techniques to remove any small unwanted objects.

The evaluation of the results of the proposed method was based on the Pratt Figure of Merit and it was also used to compare them with the results of Wen et al. and Lo et al. In conclusion, the results of the proposed method were better than the other two techniques and the researchers support that is because this method handles the noise better. After the final results researchers decided to further improve

the proposed algorithm by applying a bilateral enhancer before thresholding the image. The main disadvantage of this algorithm is that it is not flexible as it is just the capillary radius that can be adjusted for every image.

Another approach attempting to enhance the contrast between the background of the image and the capillaries was that of J. C. Riaño-Rojas, F. A. Prieto-Ortiz, L. J. Morantes, E. Sánchez-Camperos and F. Jaramillo-Ayerbe in *"Segmentation and Extraction of Morphologic Features from Capillary Images"* [22]. The method researchers proposed consists of three steps: improving image illumination, highlighting enhancement and finally smoothing of the image. What separates this proposal from others is that it uses different colour spaces in order to accomplish each of the steps mentioned above. In particular, the Y component which represents the luma information in YIQ, is used to improve the illumination. Respectively, the S component which represents the saturation information in HSV, is used to improve the contrast of the image. Afterwards the images are processed by using a Wiener filter with a kernel size of 15x15 to reduce the noise and to smooth the image. Finally, the researchers extracted the components M, A and Cr from the colour spaces CMY, Lab and YCbCr and combined them into a new image which had increased contrast.
Another thing that makes this approach interesting is that the researchers proceed to the feature extraction of the capillaries. The features they focused on were: Tortuosity, width, height, density of the capillaries, the area, the perimeter, the orientation and the polarity. From these features only tortuosity was used to automatically classify the detected capillaries. Their final results were compared to images who had been manually annotated by a dermatologist and they concluded that their results were satisfactory. However, one downside of this method is that it is extremely complex which has an impact on the run time of the application making it unusable in real life situations.

A more recent and most promising paper that came up during the bibliographic research was *Robust Nailfold Capillary Skeleton Extraction*

by Niraj P. Doshi, Gerald Schaefer and Arcangelo Merla [20]. The researchers focused on improving the skeletonisation of the capillaries which is very useful during a feature extraction. Using their earlier work they decided to use a bilateral filter to reduce the image noise and then they applied histogram equalization to enhance its contrast. Finally, a Difference of Gaussians (DoG) filter was applied in order to correct the illumination of the images. The pre-processing step was followed by thresholding by using Otsu's method to binarise the image. Then, in order to remove any small unwanted objects they filtered the images with a median filter, twice.

Moving on to the skeletonisation of the capillaries, the researchers used 8-pixel connectivity as it regards pixels whose edges are attached as neighbours; and thus is able to preserve the curvature of the capillaries. Then a two-step algorithm is applied iteratively, until the following two conditions are meet.

- C(p)=1,

- $2 \leq N(p) \leq 3$

- One of the following

  - $(p_2 \vee p_3 \vee p_5) \vee p_4 = 0$, in odd iterations,

  - $(p_6 \vee p_7 \vee p_1) \wedge p_8 = 0$, in even iterations,

where, p_2, p_4, p_6 and p_8 neighbour on the edges of the pixel and p_1, p_3, p_5 and p_7 neighbour diagonally. C(p) is the number of white pixels in the selected pixel's neighbourhood. Finally, N(p) is defined as

$$N(p) = min(N_1(p), N_2(p))$$

where:

$$N_1(p) = (p_1 \vee p_2) + (p_3 \vee p_4) + (p_5 \vee p_6) + (p_6 \vee p_7)$$
$$N_2(p) = (p_2 \vee p_3) + (p_4 \vee p_5) + (p_6 \vee p_7) + (p_8 \vee p_1)$$

When these conditions are true for every pixel of the image then the algorithm can no longer remove any other pixels and the final result is acquired.

The final results of this proposal were very good compared to others that also focused on the skeletonisation of the capillaries when the detected capillaries matched the early or active Scleroderma patterns. Unfortunately that was not the case for the capillaries with characteristics of the late SD pattern which is the main disadvantage of this method.

More recent suggestions have utilized machine learning techniques in order to process the capillaroscopy images. A prime example of this is the work of R Nivedha, M Brinda, K V Suma and Bheemsain Rao *"Classification of nailfold capillary images in patients with hypertension using non-linear SVM"* [23]. Their approach consists of the following steps:

- *Colour channel selection:* As many other researches on the subject, the authors chose to work using only the green channel of the acquired image.

- *Histogram equalization:* In order to further increase the contrast of the image, the researchers applied the Adaptive Histogram Equalisation (AHE)

- *Gaussian filtering of the image:* A series of filters is tried out in order to reduce the image noise. After testing the Gaussian, mean, median, adaptive median, alpha trimmed mean, wiener and Laplacian filters, the researchers decided to use the Gaussian one as it performed the best.

- *Image binarisation with Otsu's method:* As there are multiple approaches when it comes to image segmentation, the researchers decided to test Otsu's thresholding, Region growing, Fuzzy C Means, Watershed and K means and found out that Otsu's method by far outperformed the rest.

- *DWT for feature extraction:* Discrete Wavelet Transform was uti-

lized in order to perform the feature extraction. The researchers chose to calculate the following 12 features: contrast, entropy, correlation, RMS, energy, variance, homogeneity, smoothness, mean, kurtosis, standard deviation and skewness.

- *PCA for dimensionality reduction:* A common step when using machine learning techniques in image processing is the Principal Component Analysis. Its main purpose is to eliminate any unnecessary features e.g variables which are not independent.

- *SVM for classification of the vessels:* The final step of this method is the classification of the identified capillaries. For this purpose, the authors utilized the Support Vector Machine (SVM), which is a common learning algorithm. As in most real-life applications, the samples can't be separated by using straight lines, thus the authors employed Feature Mapping which is a non-linear technique.

One of the things that separates this proposal from all the above mentioned ones is the unique choice of features. The authors chose to exclude common features mentioned in other papers which are usually used by physicians when evaluating a capillaroscopic image and instead calculated new ones.

3.2 Techniques used for similar applications

Besides searching for other proposed methods regarding nailfold capillaroscopic images, we also looked for other approaches which had similar topics as NC. These included the detection of the blood vessels or neurons whose imaging is acquired through processes similar to capillaroscopy.

One of the approaches that stood out was that of Alejandro F. Frangi, Wiro J. Niessen, Koen L. Vincken and Max A. Viergever, "Multiscale vessel enhancement filtering" [24]. The researchers used images acquired in 2d digital subtraction angiography (DSA) and MRI screening of the aortoiliac artery and the cerebral as their testing data and their goal was to identify and enhance vessels, generally described as tubular shapes, in order to improve the segmentation results. The proposed

method is based on Hessian filtering as the eigenvalues of a Hessian matrix can be used to determine the likelihood of a vessel been present. In particular, the Taylor expansion in the neighborhood of a point x_0 was used in order to model the local behaviour of an image. This is described by the following equation:

$$L(x_0 + \delta x_{0,s}) \approx L(x_{0,s}) + \delta x_0^\intercal \nabla_{o,s} + \delta x_0^\intercal H_{o,s} \delta x_0$$

where $\nabla_{o,s}$ is the gradient vector and $H_{o,s}$ is the Hessian matrix computed at x_0 at scale s.
The differential operators of L were calculated as the convolution with derivatives of Gaussians

$$\frac{\partial}{\partial x} L(x, s) = s^\gamma L(x) * \frac{\partial}{\partial x} G(x, s)$$

with the Gaussian been defined as:

$$G(x, s) = \frac{1}{\sqrt{(2\pi s^2)}} e^{-\frac{x^2}{2x^2}}$$

where γ is used for normalization purposes.
For every image a set of two eigenvalues was calculated based on which the researchers classified the vessel that was detected.

λ_1	λ_2	Orientation pattern
N	N	Noisy, no preferred direction
L	H-	Tubular structure (bright)
L	H+	Tubular structure (dark)
H-	H-	Blob-like structure (bright)
H+	H+	Blob-like structure (dark)

Table 3.1: Table of orientation patterns

35

where H: high value, L: low value, N:noisy, +/-: sign of eigenvalue

A vesselness function is used to assign a probability value the calculated features and is defined as follows:

$$V_0(s) = \begin{cases} 0, & \text{if } \lambda_2 > 0 \\ exp(-\dfrac{\lambda_1^2}{2\beta^2\lambda_2^2})(1 - exp - \dfrac{s^2}{2c^2}) \end{cases}$$

Finally, a series of calculations is performed for different scale values and the final value for vesselness is selected based on the following formula:

$$V_0(\gamma) = max_{s_{min} < s < s_{max}} V_0(s, \gamma)$$

One of the very interesting aspects of this approach is that it uses a measurement scale as it takes into consideration the fact that vessels have varying sizes. Another advantage of this method is that the final results show a good segmentation outcome and a reduction of noise in the image. Furthermore, when compared to other approaches which also use the Hessian matrix as their basis, the results show significant improvement making this approach very promising.

Another interesting work is that of Shijian Lu, Jiang Liu, Joo Hwee Lim, Zhuo Zhang, Tan Ngan Meng, Wing Kee Wong, Huiqi Li and Tian Yin Wong in *"Automatic fundus image classification for computer-aided diagnosis"* [25]. The aim of the researchers was to develop an algorithm which would successfully classify fundus images despite the wide range of diversity. As that was a very difficult task, they focused on being able to identify the normal images and point out any abnormal ones for further processing. This way they were able to use more generic image characteristics, for example smoothness, for a successful classification.

For their proposal, the researchers used the idea of range images which means that the value of the pixels expresses the distance between a known reference frame and a visible point in the scene. So, the

first step of their approach was to calculate a series of range images from each eye fundus, each having different resolution, based on the following equation:

$$R(x, y, w_i) = max(I(x, y, w_i)) - min(I(x, y, w_i))$$

where x,y are the coordinates of each pixel of the image and w_i is the size of the i-th window used to extract the range image.
The histogram of each acquired image is then calculated and its features are used for the classification of the original image. In particular, these features included the histogram mean (M), histogram variance (V) and histogram energy (E). The feature vector (FV) of each image was finally obtained

$$FV = [M_1 V_1 E_1, ..., M_i V_i E_i, ..., M_n V_n E_n]$$

where i denotes the local histogram.
Fisher's linear discriminant (FLD) was used to classify the images based on the feature vector that was calculated earlier.
In general, this proposal performs very well and has the potential to exceed a 96% accuracy as the window size reduces. However, once it reaches a size of 6, the accuracy no longer increases. Another factor that affects the level of accuracy of the method is the number of range images calculated. Once again, as their number increases, the accuracy also grows. This however is a disadvantage of the method as the increase of range images will seriously affect the execution time. On that note, the researchers suggest as future work the addition of a feature elimination stage in the overall process and the utilization of more distinct histogram features.

Another method that bears high resemblance to the processing of capillaroscopic images is that of Masoud Aghamohamadian-Sharbaf, Hamid Reza Pourreza and Touka Banaee in *"A Novel Curvature-Based Algorithm for Automatic Grading of Retinal Blood Vessel Tortuosity"*.

The authors of the paper, after testing already proposed algorithms
for the measurement of a vessel's tortuosity and pinpointing the main
disadvantages, proceeded to develop a new algorithm which is based
on the calculation of the curvature of a vessel.
The parametric representation of the curvature they used is:

$$\kappa = \frac{y\prime\prime(t)x\prime(t) - x\prime\prime(t)y\prime(t)}{(x\prime(t)^2 + y\prime(t)^2)^{3/2}}$$

As the discrete model of curvature has a high computational complex-
ity, the authors suggested a series of modifications in order to maintain
the simplicity of the proposed algorithm.
The basic steps of the proposed algorithm were the following:

- *Detection of the blood vessel of the retina:* Randon transform was
  used to extract a vessel map of the image.

- *Skeletonisation of the vessel*: Morphological thinning was applied
  on the detected vessel in order to extract its skeleton.

- *Cross-section removal:* Using a circle on every point of the skeleton
  the algorithm counts the number of crossovers and bifurcations
  and if they exceed 3 they have to be removed.

- *Calculation of the tortuosity locally and globally:* The local tortu-
  osity of every point in the skeleton of the vessel is calculated and
  their mean value are used as the global tortuosity of the image.

Some of the main advantages of this proposal were that the algorithm
is simple and thus has a fast execution time as well as the fact that the
definition of tortuosity used by the researchers is the same as the one
physicians use for the evaluation of the retina blood vessel, making it
extremely useful.

Chapter 4

Technical Background

In this chapter of the thesis we will present some theoretical background on techniques that were used for the development of the system.

4.1 Difference of Gaussian (DoG) filtering

In order be able to use thresholding techniques for the segmentation, it is important to have a uniform background in the images. For this reason we chose to apply a Difference of Gaussian filter to the capillaroscopic images.

The DoG filter is widely used in image processing for edge detection. Similarly to the Laplacian of Gaussian (LoG) filter and the Difference of Boxes (DoB) filter, it works as a two phase process. First, the filter performs a Gaussian blur on the original image using a standard deviation of σ_1. Then the filter performs a second Gaussian blur on the original image using a standard deviation of σ_2, which is usually sharper than the σ_1. The two resulting blurred images are then subtracted from each other giving the final image. For each pixel of the final image we inspect for zero-crossings. These correspond to edges of the image or to pixels that vary significantly from their neighbour. As the difference between two different low-pass filters, the DoG filter is a band-pass filter. This way, it is able to remove high frequency components of the image , e.g. noise, as well as low frequency components, e.g. homogeneous areas of images. Some of its main advantages in-

clude the robustness of the filter to noise as well as the fact that it has a very fast implementation algorithm.

The Difference of Gaussian filter is defined as:

$$h(x, y) = \frac{1}{2\pi}[\frac{1}{\sigma_1^2}exp(-\frac{x^2+y^2}{\sigma_1^2}) - \frac{1}{\sigma_2^2}exp(-\frac{x^2+y^2}{\sigma_2^2})] \qquad , where \quad \sigma_1 < \sigma_2$$

Bellow follows a schematic of the 2d filter
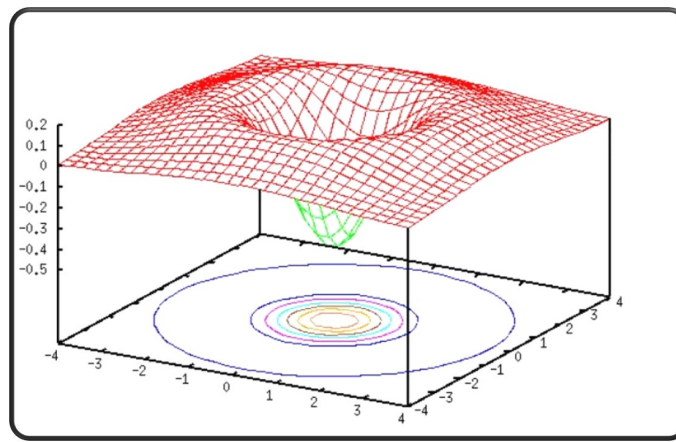
Figure 4.1: Difference of Gaussians (DoG) filter [6]

4.2 Contrast Limited Adaptive Histogram Equalisation (CLAHE)

In order to further improve the quality of the image we also used the Contrast Limited Adaptive Histogram Equalisation (CLAHE) method. CLAHE is a popular option in the image processing field, in particular in medical imaging applications. The reason for this is that CLAHE is able to intensify small details better than other enhancing techniques, which can be critical in a medical image.

CLAHE falls under the category of non-linear enhancing techniques which are based on histogram equalization. The basic idea behind histogram equalization as a contrast enhancement method is that as the multitude of pixels with a specific greyscale value increases, it should be assigned a larger part of the grey ranges available. As a result, the histogram after the equalization is almost flat.

Another benefit of choosing CLAHE over other histogram equalization

technique is that it can prevent noise amplification in homogeneous areas [26]. The way CLAHE works is the following:

Firstly the image is divided in large same size sections and the histogram of each section is calculated. Then for every pixel in the subsections, the amplification value is based on the slope of the cumulative distribution function (CDF), which is limited. The reason for this is that only a predetermined number of pixels can lay in each bin of the histogram. The allowed number of pixels, known as clip limit β, is set as a multiple of the average histogram values. This is described by the following equation

$$\beta = \frac{MN}{L}(1 + \frac{a}{100}(s_{max} - 1))$$

where, β is the clip limit, MxN the number of pixels in each image segment, L is the number of greyscale values, a is the clipping factor with range between 0-100 and s_{max} is the maximum slope allowed. [27]

The pixels whose value exceeds the clip limit are then redistributed evenly over the histogram. There is a chance that this redistribution causes areas of the histogram to exceed the clip limit. If this is unwanted the redistribution is repeated until this excess is negligible.
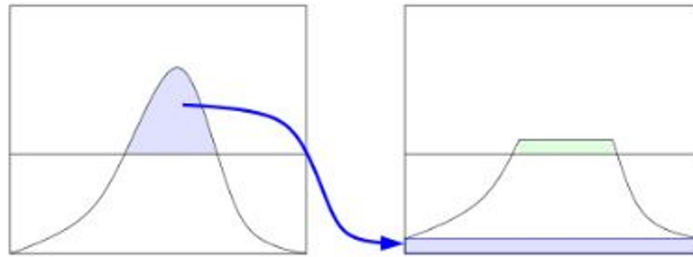
Figure 4.2: Contrast Limited Adaptive Histogram Equalization (CLAHE) [7]

4.3 Otsu Binarization Method

The main goal of thresholding in image processing is to divide the pixels of an image into distinct classes based on a selected greyscale value, the threshold value. This way the resulting image consists only from black and white pixels.

All of the binarization techniques can be classified into two classes: the

Global and the Local binarization methods. In our approach we used Otsu's Method which falls under the global binarization techniques, meaning that the threshold value that is chosen is constant over the entire image.

The Otsu binarization method was named after Nobuyuki Otsu, who was the fist to suggest this technique in 1979. The main idea of Otsu's algorihtm is to find a threshold value that maximizes between-class variance and minimizes within class variance. Then, all of the pixels of the image are classified into 2 classes using that threshold. This is described by the following equation [28]:

$$\sigma_w^2(t) = \omega_0(t)\sigma_0^2(t) + \omega_1(t)\sigma_1^2(t)$$

where, σ_0^2 and σ_1^2 are the variances of these classes and ω_0 and ω_1 weights equal to the probability of each class calculated as:

$$\omega_0(t) = \sum_{i=0}^{t-1} p(i) \quad \text{and} \quad \omega_1(t) = \sum_{i=t}^{L-1} p(i)$$

and the class means are calculated as:

$$\mu_0(t) = \frac{\sum_{i=0}^{t-1} ip(i)}{\omega_0(t)} \quad \text{and} \quad \mu_1(t) = \frac{\sum_{i=t}^{L-1} ip(i)}{\omega_1(t)}$$

and finally the intra-class variance σ_b^2 is calculated as:

$$\sigma_b^2(t) = \omega_0(t)\omega_1(t)[\mu_0(t) - \mu_1(t)]^2$$

Bellow follows a basic algorithm for the implementation of Otsu's method:

Algorithm 1 Otsu's method pseudocode [28]

1: Calculate histogram and probability of each greyscale intensity value
2: Initialize $\omega_i(0)$ and $\mu_i(0)$
3: **for** All possible threshold values $t \in [1, maxIntensity]$ **do**
4:     Calculate and update $\omega_i(0)$ and $\mu_i(0)$
5:     Calculate σ_b^2
6: **end for**
7: set threshold t= max σ_b^2

Chapter 5

Proposed Algorithmic Pipeline for Evaluation of Capillaroscopic Images

The method proposed in this thesis is based on the research paper An Improved Binarisation Algorithm for Nailfold Capillary Skeleton Extraction by Niraj P. Doshi, Gerald Schaefer and Shao Ying Zhu [29]. The researchers were able to identify the main problems of already existing methodologies and proposed an algorithm for the binarization of capillaroscopic images that tackled these problems. Our aim was to further improve on their approach and to use the resulting binary image in order to extract more structural features of the capillaries.

5.1 Image Processing

A flowchart describing the sequence of processing steps we followed for acquiring the final binary image is presented and each of the steps are then analysed in more detail.
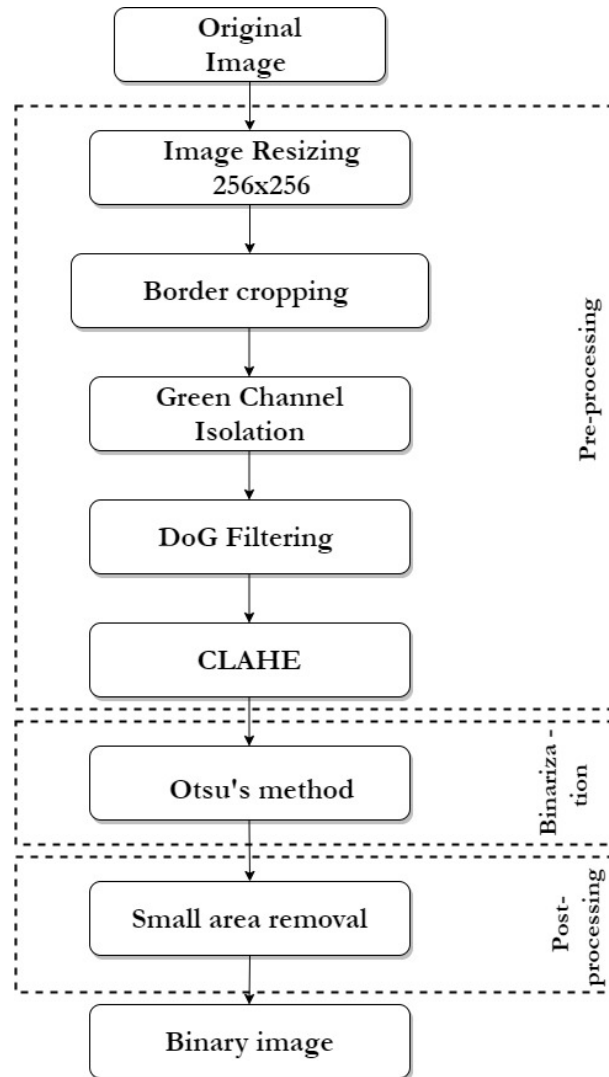
Figure 5.1: Flowchart of processing steps

5.1.1 Image Pre-processing

In order to accurately segment the images obtained during the cap-
illaroscopy procedure we have to pre-process them as they usually
suffer from inadequate contrast, lighting variations and noise. So as
to deal with those issues we used the following methods.

Image resizing and cropping

When a capillaroscopic image is inserted into the system it is resam-
pled and resized, so that the dimensions of the image are 256x256

pixels. Afterwards a 10 pixel thick border is removed from the image
in order to reduce the noise.
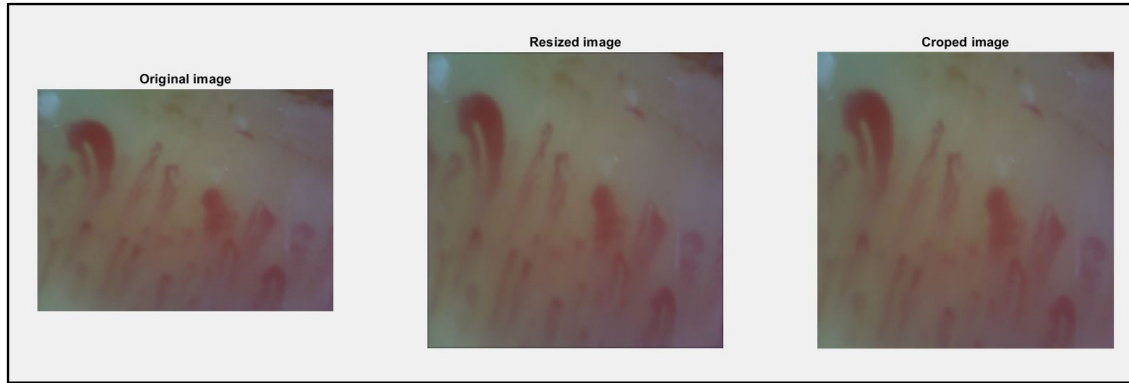
Figure 5.2: Pre-processing image results (A) Original image (B) Resized image (C)
Cropped image

Green channel isolation

Lo et al. [30] were able to prove that in the red-green-blue (RGB) capil-
laroscopic images, the green channel has the best capillary/background
contrast. Furthermore, the red and blue channels tend to be more
noisy. Using this information we chose to isolate and utilize only the
green channel of each image.
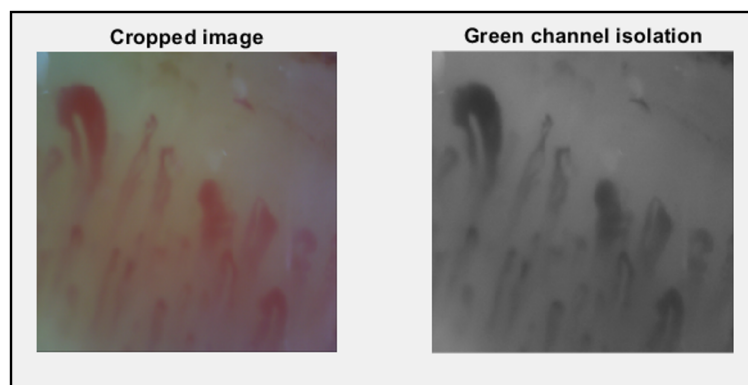
Figure 5.3: Pre-processing image results (A) Cropped image (B)Green channel isola-
tion

Difference of Gaussians (DoG) filtering

After extracting the green channel from the image, we used a DoG
filtering in order to improve the background illumination of the image

and to reduce the noise. For our approach the window size for the implementation of the filter was set to 18, while the standard deviations where set as $\sigma_2 = 4$ and $\sigma_1 = \frac{\sigma_2}{3.5}$.

Contrast Limited Adaptive Histogram Equalization (CLAHE)

In order to further improve the quality of the image before thresholding we use the Contrast Limited Adaptive Histogram Equalization (CLAHE) method.

5.1.2 Image Binarization

Otsu Binarization Method

Afterward image is binarized using Otsu's Method as described in Chapter 4. The threshold is automatically selected depending on the image selected to be processed.

5.1.3 Image Post-processing

Small area removal

In order to improve the results from Otsu's thresholding we needed to further process the image. This is also known as post processing in digital processing. For our implementation the connectivity was set to 8, meaning that two pixels are considered to be connected if their edges or corners are connected. Additionally, the minimum size of an area for not been deleted was set equal to 150 after testing it and comparing these results to those of other values.

After applying all of the above processing techniques to our images in the dataset provided, the results were the following:
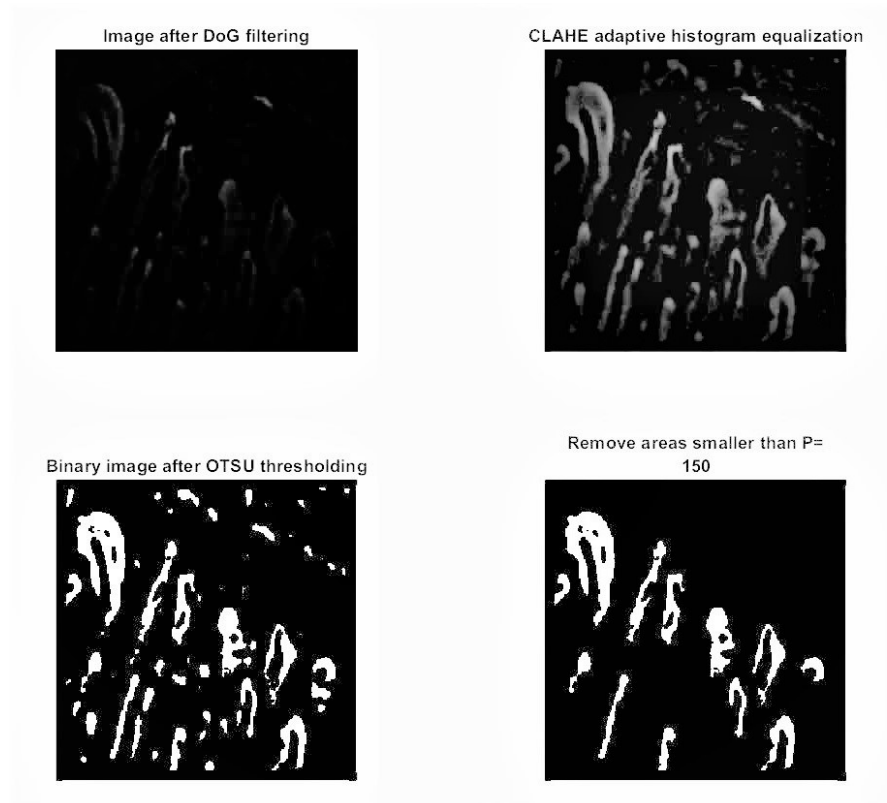
Figure 5.4: Image results after applying (A)DoG filter (B)CLAHE (C)Otsu thresholding (D)Small area removal

Finally, we appose the original image next to the final result acquired after the proposed processing method for easier comparison.
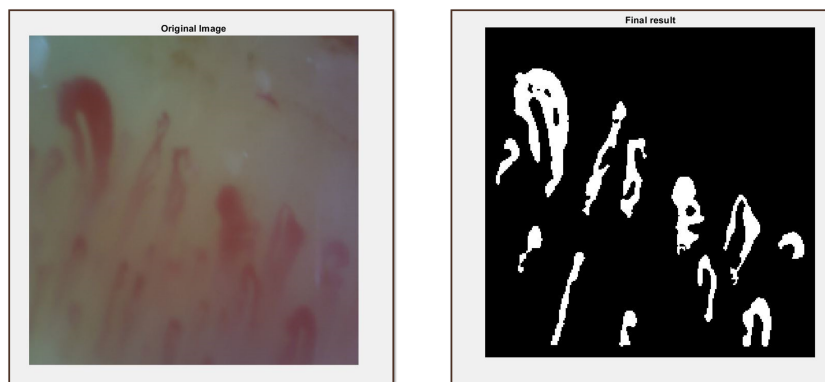
Figure 5.5: On the left, original image from dataset and on the right image after digital processing

5.2 Feature Extraction

In order to extract the necessary features from the capillaries we focused on two different levels on the image. Firstly we focused on each capillary isolated in order to acquire a set of features for each and every one of them individually. Secondly, we looked at the image as a whole and extracted a series of features representative of the capillaries.

5.2.1 Features of individual capillaries

After the segmentation of the image each capillary was extracted and stored separately in order to be processed as an individual and thus compute the desired characteristics. An overview of the processing steps and the calculations performed follows.
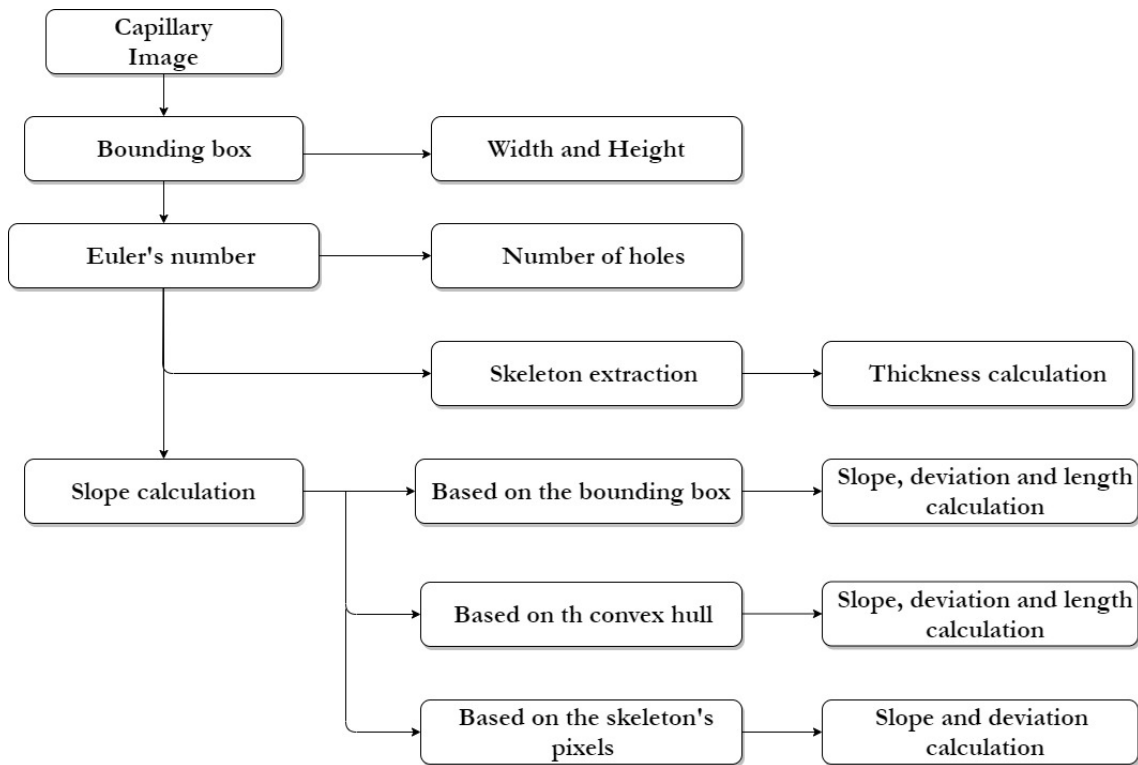
Figure 5.6: Flowchart of processing steps and calculations of individual capillaries

Height and Width of capillary's bounding box

After placing a bounding box around each capillary we calculate the width and the height of these boxes. The result of that process is the

following.
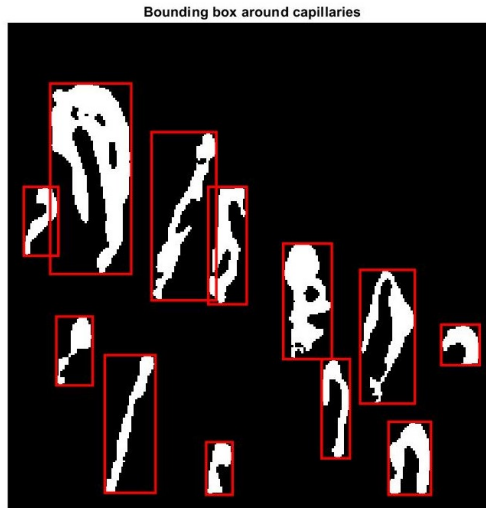
Figure 5.7: Binary image with bounding boxes around the capillaries

It is important to note that the bounding box calculated for this purpose has the same orientation as the image. A different approach will be described later when the bounding box will be utilized for the calculation of a capillary's orientation.

Number of holes in the capillary

A very useful mathematical tool for calculating the number of holes in a capillary is Euler's number, also refereed to as Euler's characteristic. It is defined as the number of objects in an image minus the total number of holes in those objects.
As we have already isolated the capillaries, the calculation is performed for each capillary separately. This feature is particularly useful to determine whether or not a capillary is twisted.

Skeleton extraction

The skeleton of any blob is defined as the mid-way between its edges. As the most commonly used techniques for the extraction of the skeleton didn't produce sufficient results we proposed the following method.
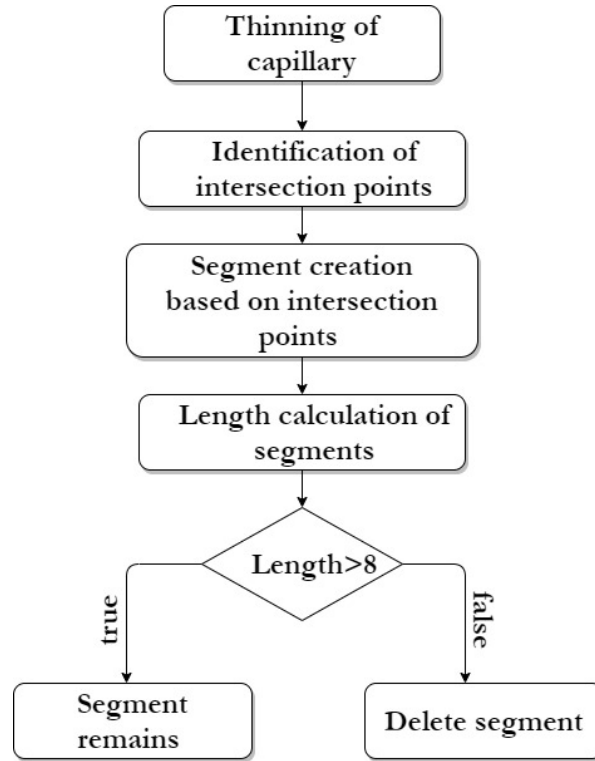
Figure 5.8: Flowchart of skeleton extraction

First a thinning of the binary image is performed and a binary image whose object is reduced to a single connected line is obtained. In order to identify the intersection points on the skeleton, e.g. pixels with more than two neighbours, we convoluted the image with the following filter h:

$$h=\begin{bmatrix} 1 & 1 & 1 \\ 1 & 0 & 1 \\ 1 & 1 & 1 \end{bmatrix}$$

Afterwards the pixels were grouped together in line segments based on the intersection points that were previously located. Finally, any branch whose length was smaller than a threshold value, in our case it was set equal to 8 pixels, is removed from the image.

Thickness of capillary
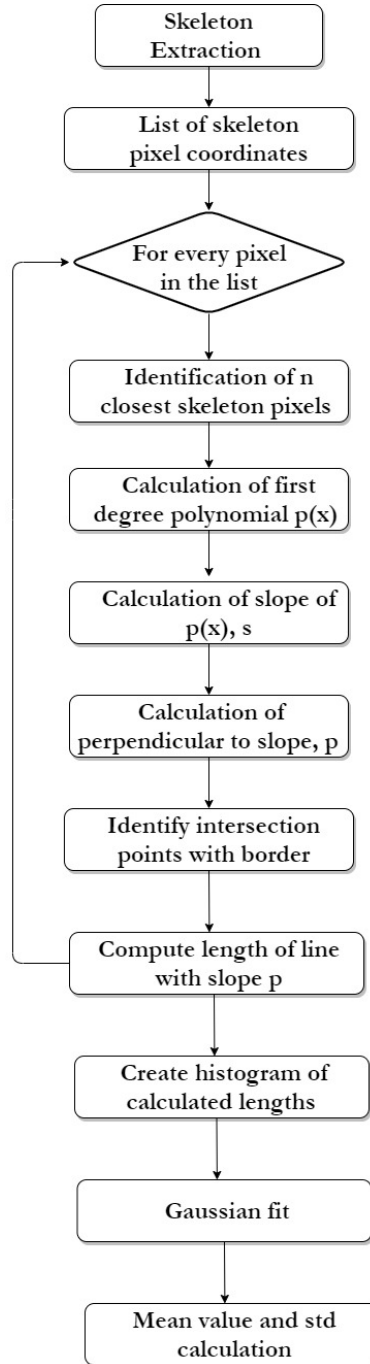
Figure 5.9: Flowchart of thickness calculation

Following the "thinning" process, we identified the 10 closest laying pixels based on the smallest calculated euclidean distances. These pixels were used to calculate the coefficients of a polynomial p(x) of first

degree, representing a line. Afterwards, the slope of the line described by the polynomial was calculated and was used as the slope of the selected pixel.

A line with direction perpendicular to the pixel's was then drawn, the endpoints of which were set as the boundary points of the capillary detected that intersected with the line. The length of that line was used as the local thickness of the vessel and the process was repeated for every pixel in the skeleton of the vessel.

A snapshot of the process described above is illustrated on the left of the following image and the final histogram of the calculated distances is on the right.
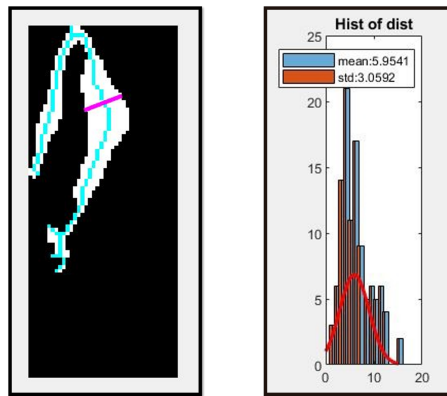
Figure 5.10: On the left, snapshot of binary image of capillary with skeleton (blue) and vertical distance calculated (magenta), and on the right histogram of the distances calculated

After calculating the the thickness for every pixel in the skeleton we then proceeded with the creation of the histogram. A Gaussian fit was later performed and the mean value and the standard deviation of the histogram were calculated.

Slope of capillary

As the slope of a capillary is not defined strictly but in a more qualitative way, we developed three different approaches in order to see which one would produce a result that could be generally accepted.

Based on the slope of its bounding box

For the first method of calculation of the slope of a capillary we firstly placed a bounding box around the capillary.
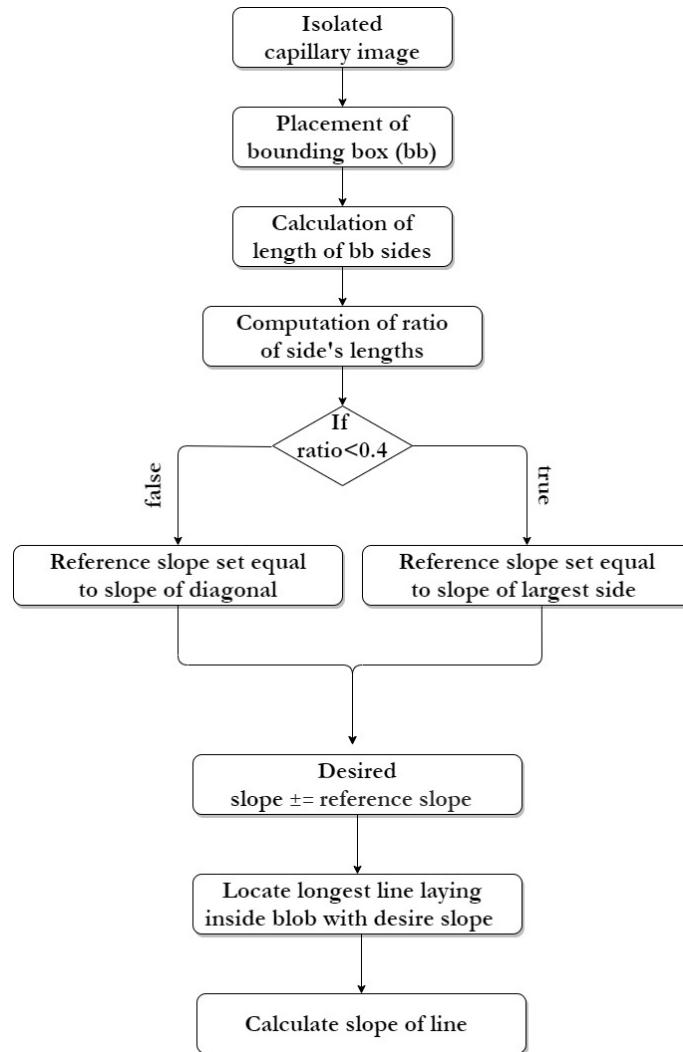
Figure 5.11: Flowchart of slope calculation based on capillary's bounding box

It is important to note that we didn't use the same method as before for the calculation of the bounding box rather we used a new one that minimizes the area of the box and allows a different orientation than the one of the image. Then the length of the sides of the bounding box were measured and their ratio was calculated. If the ratio was found smaller than 0.4 then the reference slope was set equal to the slope of the bounding box's longest side. Otherwise, the reference slope was

set equal to the slope of the diagonal of the bounding box. Finally we located the longest line that lays inside each capillary and has a slope equal to the reference slope or deviates by it by a maximum of 0.1rad. The final result of the process described above follows. Lines calculated based on the slope of the diagonal are colored blue while the ones calculated based on the longest side are colored red.
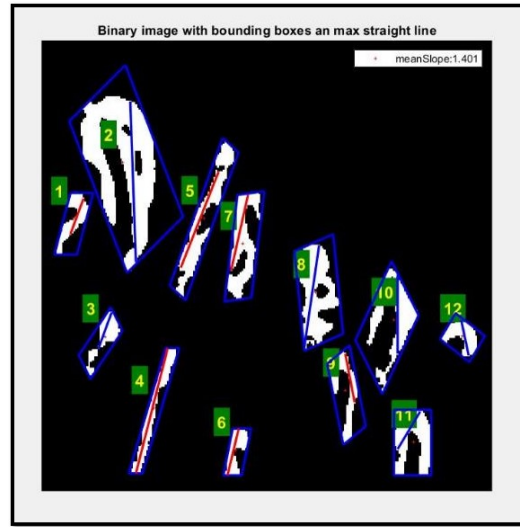
Figure 5.12: Capillaries with their bounding boxes and longest lines detected based on reference slope

Finally, a main slope is calculated for the whole image based on these slopes in a way which we will later describe. The main slope is used in order to calculate the deviation of each capillary.

Based on the slope of the maximum diameter of its convex hull

The second approach utilized for the calculation of the capillaries' slopes was based on the maximum diameter of its convex hull. A flowchart describing the basic steps of the method follows.
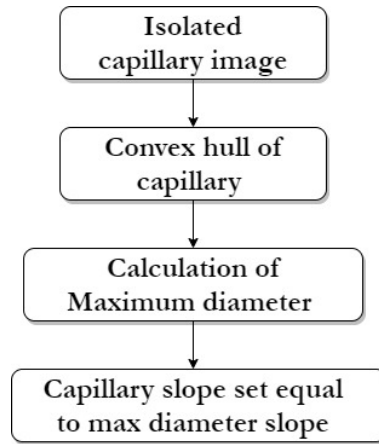
Figure 5.13: Flowchart of slope calculation based on capillary's convex hull

For this method, we first computed the convex hull of each vessel. The maximum diameter of the convex hull was then calculated and its slope represented the slope of the capillary. The convex hulls of the capillaries and their maximum diameters are illustrated bellow.
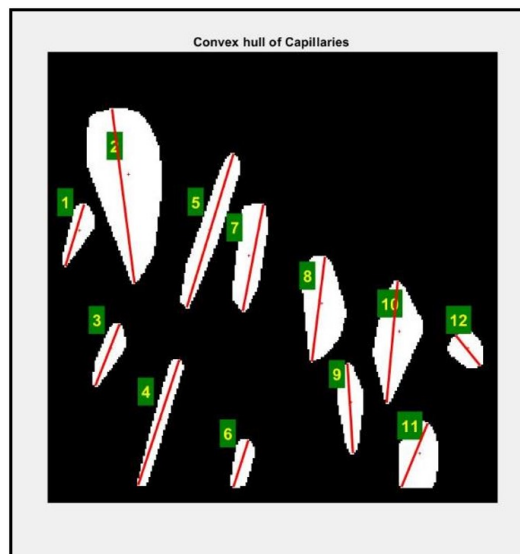
Figure 5.14: Convex hull of capillaries with maximum diameter

Finally, based on the slopes of the capillaries a main slope for the image is calculated. That main slope is then used to calculate the deviation of each capillary in the same way as the previous approach.

Based on the slopes of the pixels of the capillary's skeleton

The third method of calculation of the slope of a capillary was based on the slopes of the pixels of the capillary's skeleton. For this approach it was necessary to firstly define the following divisions of the plane:

- *The $\frac{\pi}{6}$ division:* This division separates the plane in the following segments: $[0, \frac{\pi}{12}], [\frac{\pi}{12}, \frac{3\pi}{12}], [\frac{3\pi}{12}, \frac{5\pi}{12}], [\frac{5\pi}{12}, \frac{7\pi}{12}], [\frac{7\pi}{12}, \frac{9\pi}{12}], [\frac{9\pi}{12}, \frac{11\pi}{12}], [\frac{11\pi}{12}, \pi)$
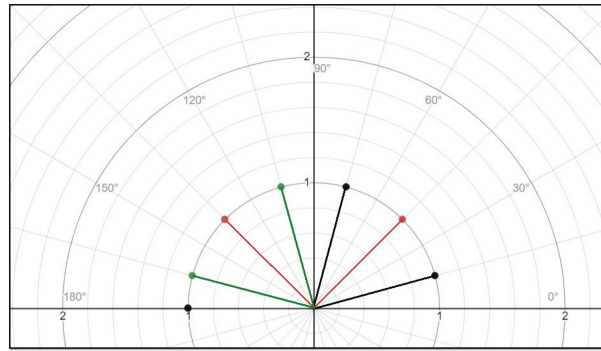
Figure 5.15: Schematic of the $\frac{\pi}{6}$ division

- *The $\frac{\pi}{4}$ division:* This division separates the plane in the following segments: $[0, \frac{\pi}{8}], [\frac{\pi}{8}, \frac{3\pi}{8}], [\frac{3\pi}{8}, \frac{5\pi}{8}], [\frac{5\pi}{8}, \frac{7\pi}{8}], [\frac{7\pi}{8}, \pi)$
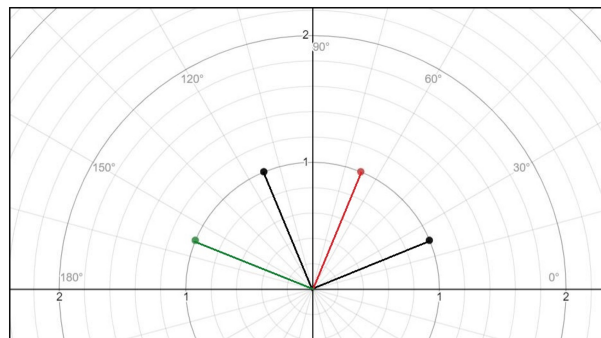
Figure 5.16: Schematic of the $\frac{\pi}{4}$ division

A flowchart describing the basic steps of our approach follows

56
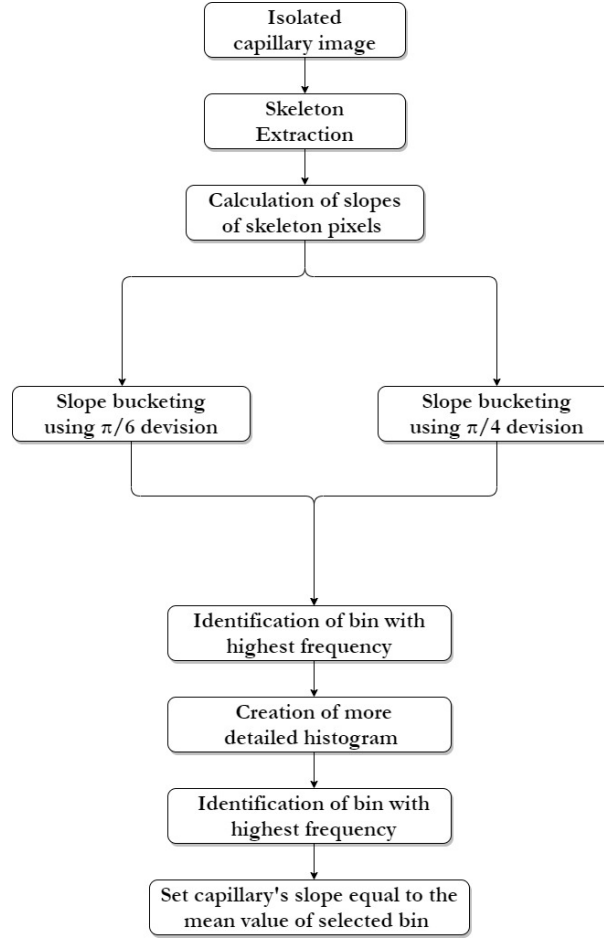
Figure 5.17: Flowchart of slope calculation based on the slopes of the pixels of the skeleton

Firstly, the slope for each pixel in the capillary's skeleton was evaluated in the same way as for the thickness calculation, however this time we used only the 3 closest pixels in order for more precision. Afterwards, the calculated slopes were bucketed using the $\frac{\pi}{6}$ and $\frac{\pi}{4}$ divisions and a histogram was created in both cases. The bin with the highest frequency was identified for both of the histograms and a second more detailed histogram in the range of the highest frequency bin was created from the slopes of the pixels of the skeleton. We then once again identified the bin with the highest frequency and the mean value was set equal to the slope of the capillary. Finally, based on the slopes of the capillaries a main slope for the image is calculated. That main slope is then used to calculate the deviation of each capillary in the same way as the previously mentioned approaches.

5.2.2 Global features of image

A set of global features is acquired from every image processed by the system. A general overview describing the processing steps that we will later explain in more detail and the calculations performed follows.
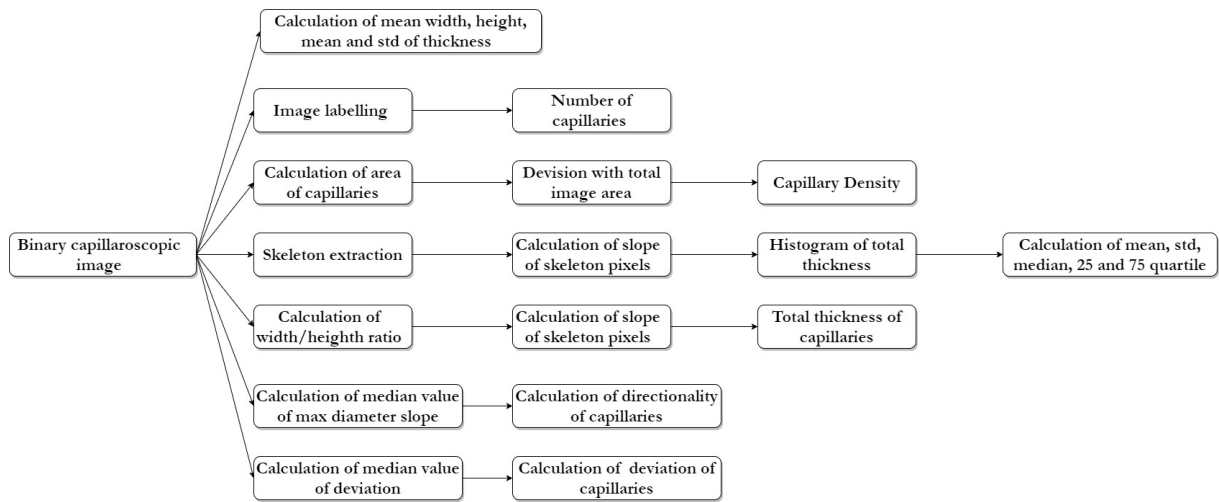
Figure 5.18: Flowchart of global feature extraction from image

Mean capillary features

For every image processed we aimed to create a representative capillary whose values could be used for a general assessment of the image. After calculating the width and the height of the bounding box of every capillary, we then computed their mean value and the results were set as the width and height of the representative capillary. The same process was repeated for determining the mean thickness and the standard deviation of that capillary.

Number of capillaries and Capillary Density

First and foremost the number of capillaries detected was calculated and then we moved on to calculate the density of the capillaries. For that purpose, we firstly calculated the area that each capillary occupied, we summed them and the result was finally divided by the total area of the image. The main reason we chose this method in order to calculate the density of the capillaries was the lack of information on

the scale used during the capillaroscopic examination in the dataset and this method provided a way to overcome that problem.

Thickness measures from all capillaries

Next we calculated a series of features regarding the thickness of the vessels of the capillaroscopic image. A flowchart describing the methodology for these calculations follows.
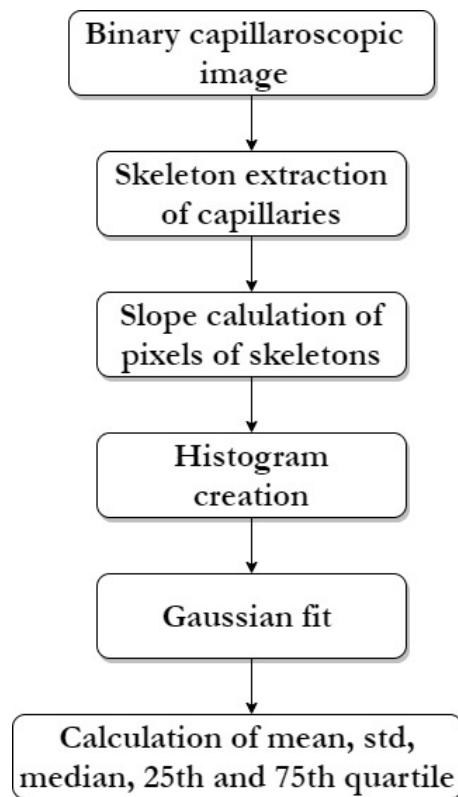
Figure 5.19: Flowchart of total thickness calculation

The skeleton of the capillaries was once again extracted and the slope of each pixel of the skeleton was calculated. A general histogram was then created from these values and a Gaussian fit was performed in order to acquire a series of features. In particular, we were interested in the mean value and the standard deviation of the histogram. Furthermore, we also computed the median value as well as the 25th and the 27th quartile in order to have an overall picture of the thickness of the capillaries.

Total thickness

A total thickness of the capillaries is calculated for the capillaroscopic images based on

$$\frac{\sum_i \dfrac{w_i}{h_i} E_i}{\sum_i |E_i|}$$

where C_i: capillary, E_i: size of Capillary, w_i: width of bounding box of capillary and h_i: height of bounding box of Capillary

Total directionality

For every image, the total directionality of the capillaries is calculated based on

$$\frac{\sum_i |a_i - a_{mean}| E_i}{\sum_i |E_i|}$$

where C_i: capillary, E_i: size of Capillary, a_{meam}: mean value of maximum diameter slope and a_i: max diameter slope

It is important to note that the mean slope we used for the calculation of this feature was the mean value of the slopes of the capillaries calculated based on the three different approaches we have already mentioned and not on the mean value of the total slope histogram. For this reason we repeated the calculation 4 times, once for the mean slope based on the bounding box of the capillary, once for the mean slope based on the convex hull of the capillary and finally twice for the mean slope calculated based on the skeleton's pixels, once for the $\frac{\pi}{6}$ division and once for the $\frac{\pi}{4}$ division. This feature is particularly useful when comparing the performance of these different approaches.

Total deviation

We define total deviation of the capillaries as

$$\frac{\sum_i |d_i - d_m| E_i}{\sum_i |E_i|}$$

where C_i: capillary, E_i: size of Capillary, d_m: mean value of deviation from main slope and d_i: deviation of capillary

The calculation of this feature is also repeated 4 times for the same reasons as the total directionality and it is also useful when comparing the performance of the approaches used for calculating the slopes of the capillaries.

Chapter 6

Results

This section of the thesis will present the performance on the dataset provided of the developed system. The initial dataset kindly provided by Professor Pancaldi Fabrizio, included 41 capillaroscopic images. After examining the images only 15 were selected for testing and the rest were disregarded as the glaring caused by the immersion oil was too intense. Out of the 15 images selected, for the sake of completeness, we chose to analytically present the results of three as each one represents a different category of potential images that the system will have to process. Unfortunately, as the level of magnification used during the capillaroscopy was not recorded, most of the results are measured using pixels as a metric unit with the exception of the slopes which are calculated in rad.

6.1 Results of image of normal capillaries

In the first image selected the capillaries present the typical pattern which is expected when examining the nailfold bed of a healthy individual. Bellow follow the results of the system's calculations.

Image Binarization Results

After following the preprocessing steps described on Chapter 4 the image is thresholded and a binary image is obtained. Each capillary

detected is annotated with a label and we will further refer to it using this number.
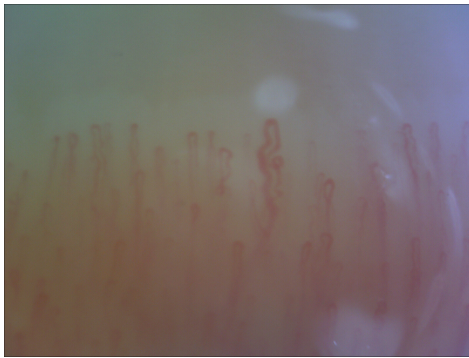
(a) Original image acquired by healthy individual.
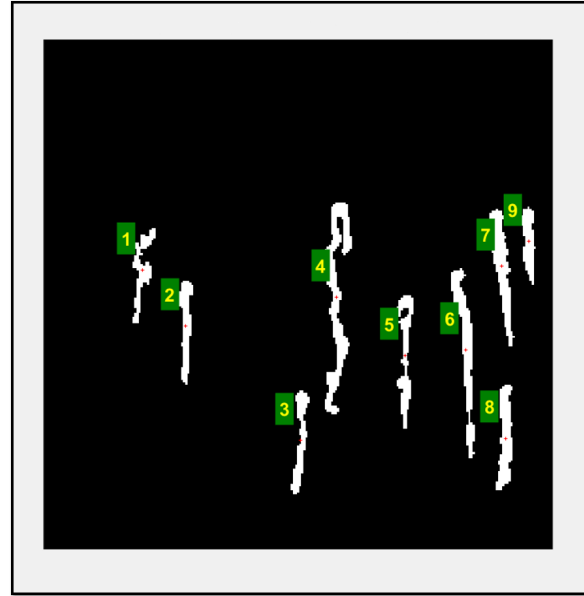
(b) Binary image with labels

6.1.1 Individual capillary measures

Basic features results

The width, the height, the number of holes, the mean thickness and the standard deviation of the thickness are the first parameters to be measured for each capillary separately. A table of the calculated features follows:

No	Width	Height	Holes	max_thick	m_thick	std_thick
1	11	45	0	6	4.7436	2.8536
2	7	49	0	6	4.7209	0.90831
3	9	49	0	5	4.4186	1.1595
4	14	100	0	7	5.9907	3.6665
5	9	63	0	6	4.7077	2.1918
6	11	90	0	6	4.9425	1.3923
7	13	65	0	7	5.7667	1.6194
8	8	50	0	7	6	1.1127
9	7	37	0	6	5.3333	1.291

Figure 6.2: Results of individual capillaries, measurements in pixels

Slope calculations

The results of all three different approaches for calculating the slope
of the capillaries are presented in the following matrices.

- Based on the slope of its bounding box

capillaryNo	bbSlope	Slope	length	deviation
1	1.47	1.54	29.51	0.05
2	1.52	1.59	48.01	0.01
3	1.52	1.52	38.05	0.07
4	1.55	1.64	62.13	0.05
5	1.55	1.54	53.53	0.05
6	1.67	1.63	80.61	0.04
7	1.7	1.68	64.38	0.09
8	1.53	1.51	49.09	0.08
9	1.63	1.63	36.06	0.04

Figure 6.3: Slope of capillaries based on their bounding boxes, in rad

- Based on the slope of the biggest diameter of its convex hull

cNo	Slope	length	deviation
1	1.35	45.12	0.19
2	1.59	48.01	0.05
3	1.49	48.17	0.05
4	1.51	99.18	0.03
5	1.52	62.07	0.02
6	1.63	89.14	0.09
7	1.68	64.38	0.14
8	1.45	49.37	0.09
9	1.63	36.06	0.09

Figure 6.4: Slope of capillaries based on their convex hull, in rad

- Based on the slopes of the pixels of the skeleton

No	mainSlope30	deviation30	mainSlope45	deviation45
1	0.85	0.58	1.35	0.28
2	1.35	0.08	1.35	0.28
3	1.35	0.08	1.35	0.28
4	1.2	0.23	1.85	0.22
5	1.55	0.12	1.55	0.08
6	1.55	0.12	1.55	0.08
7	1.55	0.12	1.85	0.22
8	1.55	0.12	1.55	0.08
9	1.55	0.12	1.55	0.08

Figure 6.5: Slope of capillaries based on the pixels of the skeleton, in rad

The above results were based on the following histograms formed
for every capillary.
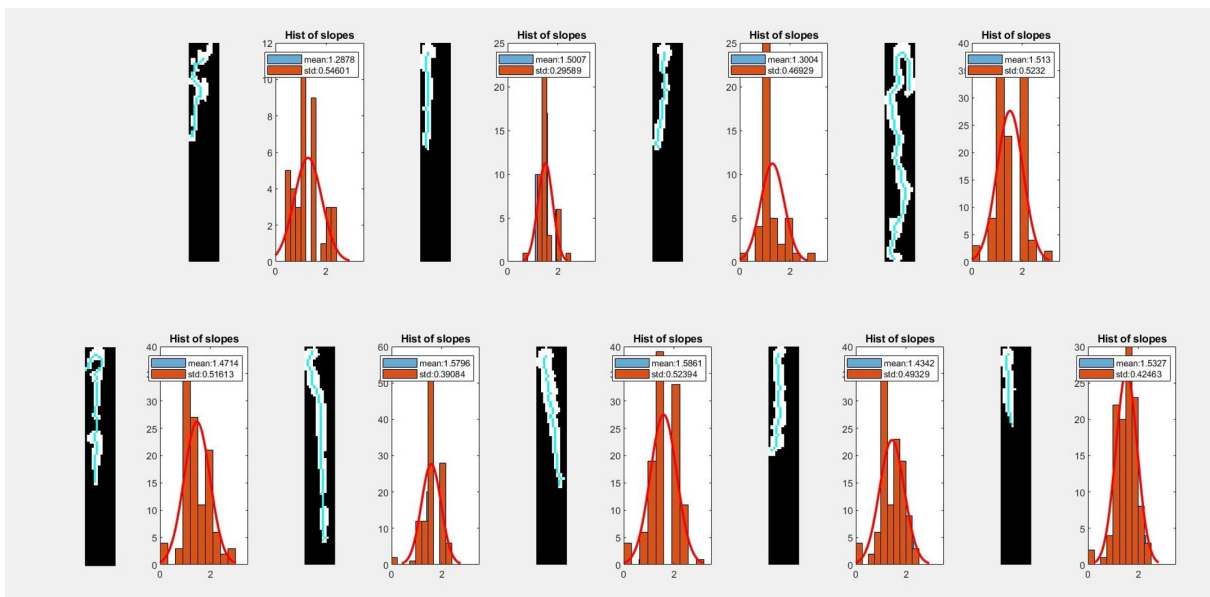
Figure 6.6: Histograms of slopes of skeleton pixels

6.1.2 Results comparison

A comparison on the results from the different approaches follows

- Slope Calculation

No	Slope30	Slope45	Bounding Box Slope	Convex Hull Slope
1	0.85	1.35	1.54	1.35
2	1.35	1.35	1.59	1.59
3	1.35	1.35	1.52	1.49
4	1.2	1.85	1.64	1.51
5	1.55	1.55	1.54	1.52
6	1.55	1.55	1.63	1.63
7	1.55	1.85	1.68	1.68
8	1.55	1.55	1.51	1.45
9	1.55	1.55	1.63	1.63

- Standard Deviation

No	Slope30	Slope45	Bounding Box Slope	Convex Hull Slope
1	0.58	0.28	0.05	0.19
2	0.08	0.28	0.01	0.05
3	0.08	0.28	0.07	0.05
4	0.23	0.22	0.05	0.03
5	0.12	0.08	0.05	0.02
6	0.12	0.08	0.04	0.09
7	0.12	0.22	0.09	0.14
8	0.12	0.08	0.08	0.09
9	0.12	0.08	0.04	0.09

6.1.3 Total Image Results

For the image as a total, the features calculated were the following:

Total image results

totalCapillaries	Density	Thickness
9	0.31966	0.16225

Figure 6.7: Total measures of the image, in pixels

Mean Capillary Results

m_width	m_height	m_mthick	std_thick
9.8889	60.889	5.1804	1.7995

Figure 6.8: Total measures of mean capillary of the image, in pixels

Total width histogram from all capillaries

Hist_mean	Hist_std	Hist_median	Hist_25quartile	Hist_75quartile
5.2596	2.2968	5	4.7143	5.8787

Figure 6.9: Total measures of histogram of the image, in pixels
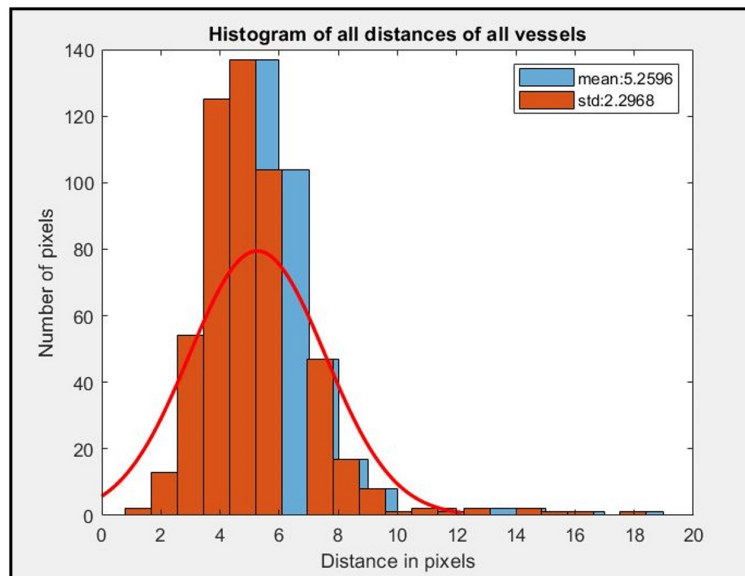
Figure 6.10: Width histogram from all capillaries, in pixels

6.1.4 Total slope and total deviation

Finally, the total slope and the total deviation for the capillaries in the
image are calculated:

- Based on the slope of its bounding box

totalSlope	totalDeviation
1.59	0.05

Figure 6.11: Total slope and total deviation based on the slope of its bounding box,
in rad

- Based on the slope of the biggest diameter of its convex hull

totalSlope	totalDeviation
1.54	0.08

Figure 6.12: Total slope and total deviation based on the biggest diameter of its convex hull, in rad

- Based on the slopes of the pixels of the skeleton

totalSlope30	totalDeviation30	totalSlope45	totalDeviation45
1.43	0.14	1.63	0.17

Figure 6.13: Total slope and total deviation based on the slopes of the pixels of the skeleton, in rad

6.2 Results of image of normal and abnormal capillaries

In the second image there is presence of both normal and abnormal capillaries. Bellow follow the results of the system's calculations.

Image Binarization Results

After following the preprocessing steps described on Chapter 4 the image is thresholded and a binary image is obtained. Each capillary detected is annotated with a label and we will further refer to it using this number.
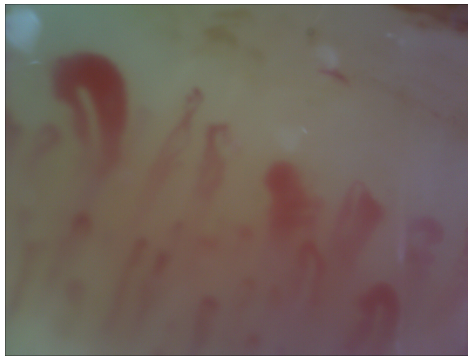
(a) Original image acquired by healthy individual.
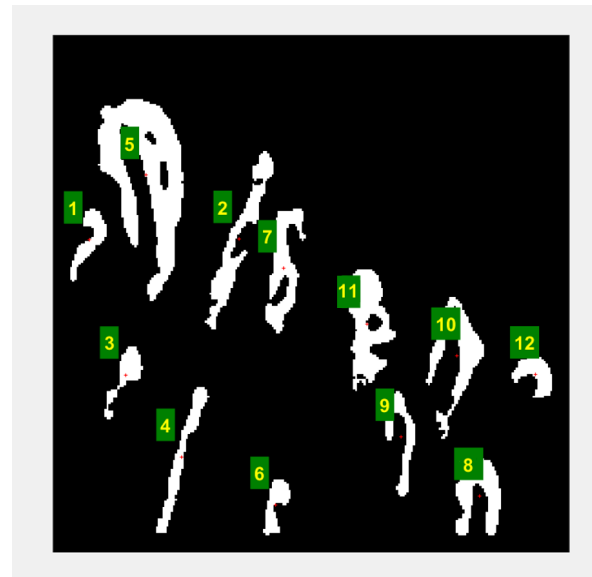
(b) Binary image with labels

6.2.1   Individual capillary measures

Basic features results

The width, the height, the number of holes, the mean thickness and the standard deviation of the thickness are the first parameters to be measured for each capillary separately. A table of the calculated features follows:

No	Width	Height	Holes	max_thick	m_thick	std_thick
1	17	34	0	7.5	6.963	4.4849
2	27	66	0	7	5.8387	2.8753
3	21	36	0	9	7.6667	2.2654
4	19	20	0	10	7.7407	2.943
5	40	94	4	15.5	12.263	8.0388
6	18	34	0	11	6.037	3.7671
7	25	68	0	6	5.2295	1.0391
8	32	83	0	9	6.8228	2.8679
9	13	26	0	7	6.25	2.0166
10	19	58	0	8	8.1013	5.502
11	24	57	2	20	14.418	9.7657
12	14	49	0	6	4.8929	1.4731

Figure 6.15: Results of individual capillaries, measurements in pixels

Slope calculations

The results of all three different approaches for calculating the slope
of the capillaries are presented in the following matrices.

- Based on the slope of its bounding box

capillaryNo	bbSlope	Slope	length	deviation
1	1.32	1.22	20.25	0.18
2	1.58	1.61	86.05	0.2
3	1.29	1.22	20.76	0.18
4	1.28	1.32	69.12	0.08
5	1.23	1.2	55.31	0.21
6	1.37	1.34	25.71	0.07
7	1.45	1.35	41.47	0.05
8	1.33	1.43	55.58	0.03
9	1.77	1.76	26.48	0.36
10	1.5	1.57	42	0.17
11	1.05	1.03	23.32	0.37
12	1.85	1.78	19.42	0.38

Figure 6.16: Slope of capillaries based on their bounding boxes, in rad

- Based on the slope of the biggest diameter of its convex hull

cNo	Slope	length	deviation
1	1.28	34.48	0.17
2	1.7	93.77	0.26
3	1.2	35.47	0.25
4	1.25	70.52	0.19
5	1.27	85.73	0.17
6	1.26	26.25	0.18
7	1.38	58.05	0.06
8	1.45	56.44	0
9	1.63	48.09	0.19
10	1.48	65.28	0.03
11	1.18	36.77	0.26
12	2.25	20.62	0.81

Figure 6.17: Slope of capillaries based on their convex hull, in rad

- Based on the slopes of the pixels of the skeleton

No	mainSlope30	deviation30	mainSlope45	deviation45
1	1.05	0.55	1.05	0.45
2	1.25	0.35	1.25	0.25
3	1.15	0.45	1.35	0.15
4	1.85	0.25	1.35	0.15
5	2.1	0.5	1.75	0.25
6	1.15	0.45	1.75	0.25
7	1.25	0.35	1.25	0.25
8	1.15	0.45	1.15	0.35
9	1.15	0.45	1.15	0.35
10	1.15	0.45	1.55	0.05
11	1.85	0.25	1.55	0.05
12	1.55	0.05	1.55	0.05

Figure 6.18: Slope of capillaries based on the pixels of the skeleton, in rad

The above results were based on the following histograms formed for every capillary.
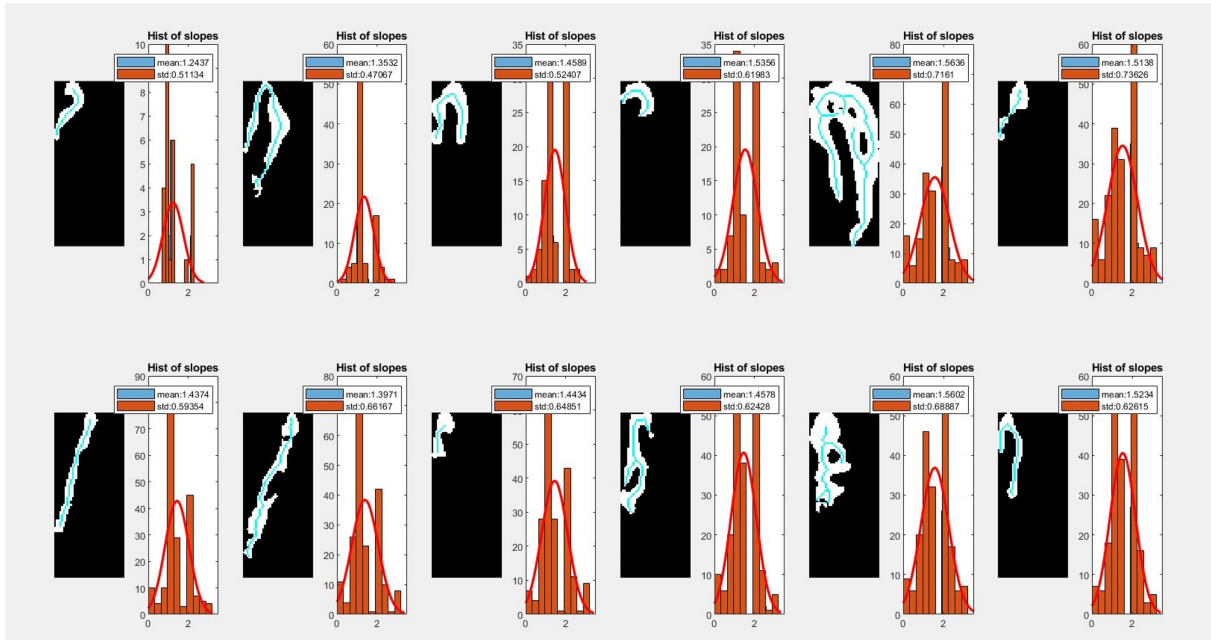
Figure 6.19: Histograms of slopes of skeleton pixels

6.2.2 Results comparison

A comparison on the results from the different approaches follows

- Slope Calculation

No	Slope30	Slope45	Bounding Box Slope	Convex Hull Slope
1	1.05	1.05	1.22	1.28
2	1.25	1.25	1.61	1.7
3	1.15	1.35	1.22	1.2
4	1.85	1.35	1.32	1.25
5	2.1	1.75	1.2	1.27
6	1.15	1.75	1.34	1.26
7	1.25	1.25	1.35	1.38
8	1.15	1.15	1.43	1.45
9	1.15	1.55	1.76	1.63
10	1.15	1.15	1.57	1.48
11	1.85	1.55	1.03	1.18
12	1.55	1.55	1.78	2.25

- Standard Deviation

No	Slope30	Slope45	Bounding Box Slope	Convex Hull Slope
1	0.55	0.45	0.18	0.17
2	0.35	0.25	0.2	0.26
3	0.45	0.15	0.18	0.25
4	0.25	0.15	0.08	0.19
5	0.5	0.25	0.21	0.17
6	0.45	0.25	0.07	0.18
7	0.35	0.25	0.05	0.06
8	0.45	0.35	0.03	0
9	0.45	0.35	0.36	0.19
10	0.45	0.05	0.17	0.03
11	0.25	0.05	0.37	0.26
12	0.05	0.05	0.38	0.81

6.2.3 Total Image Results

For the image as a total, the features calculated were the following:

Total image results

totalCapillaries	Density	Thickness
12	0.29993	0.41741

Figure 6.20: Total measures of the image, in pixels

Mean Capillary Results

m_width	m_height	m_mthick	std_thick
22.417	52.083	7.6853	3.9199

Figure 6.21: Total measures of mean capillary of the image, in pixels

Total width histogram from all capillaries

Hist_mean	Hist_std	Hist_median	Hist_25quartile	Hist_75quartile
8.5621	6.3399	7	5.9379	7.921

Figure 6.22: Total measures of histogram of the image, in pixels
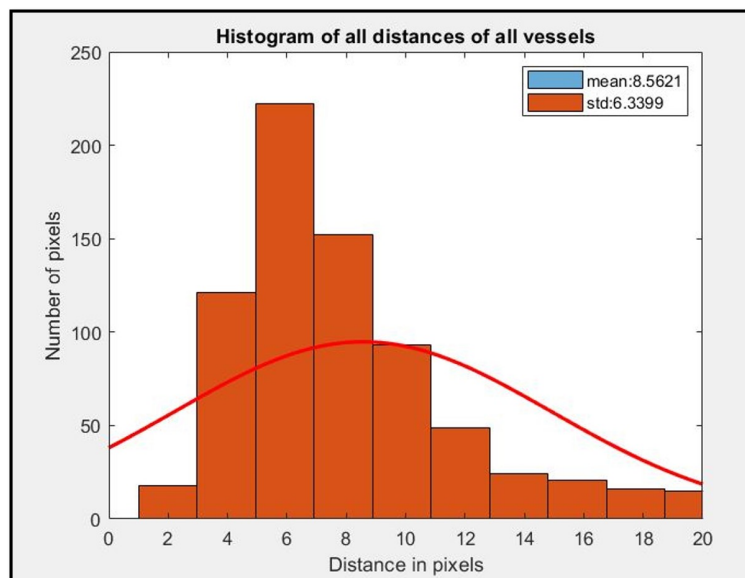
Figure 6.23: Width histogram from all capillaries, in pixels

6.2.4 Total slope and total deviation

Finally, the total slope and the total deviation for the capillaries in the image are calculated:

- Based on the slope of its bounding box

totalSlope	totalDeviation
1.4	0.19

Figure 6.24: Total slope and total deviation based on the slope of its bounding box, in rad

- Based on the slope of the biggest diameter of its convex hull

totalSlope	totalDeviation
1.44	0.21

Figure 6.25: Total slope and total deviation based on the biggest diameter of its convex hull, in rad

- Based on the slopes of the pixels of the skeleton

totalSlope30	totalDeviation30	totalSlope45	totalDeviation45
1.6	0.4	1.5	0.2

Figure 6.26: Total slope and total deviation based on the slopes of the pixels of the skeleton, in rad

6.3 Results of image of abnormal capillaries

In the third image it is obvious that there have been severe alterations on the structure of the capillaries. Bellow follow the results of the system's calculations.

Image Binarization Results

After following the preprocessing steps described on Chapter 4 the image is thresholded and a binary image is obtained. Each capillary detected is annotated with a label and we will further refer to it using this number.
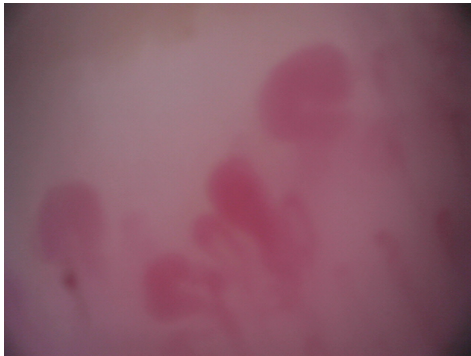
(a) Original image acquired by healthy individual.
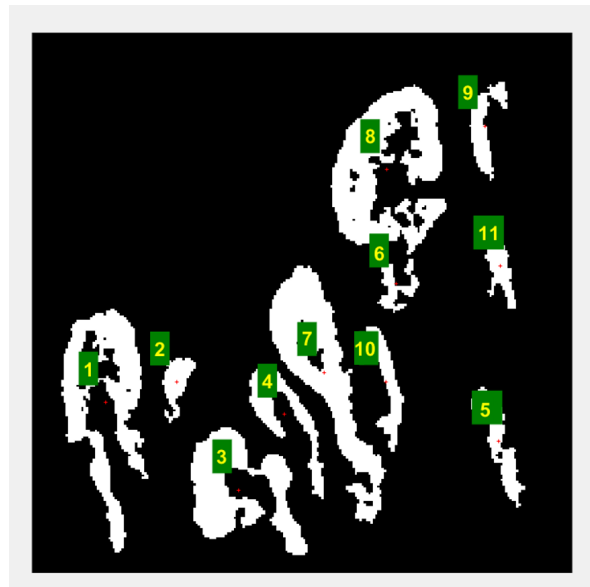
(b) Binary image with labels

6.3.1 Individual capillary measures

Basic features results

The width, the height, the number of holes, the mean thickness and the standard deviation of the thickness are the first parameters to be measured for each capillary separately. A table of the calculated features follows:

No	Width	Height	Holes	max_thick	m_thick	std_thick
1	39	109	4	12	9.9552	6.3287
2	24	54	1	11	8.8846	5.208
3	14	39	0	10	8.2143	5.8914
4	15	29	0	11	8.12	3.3332
5	52	57	1	15	13.702	10.398
6	33	60	0	10	7.3108	3.955
7	52	115	2	16	14.46	10.283
8	52	76	9	19	14.889	9.3083
9	19	56	0	11	7.2245	2.1435
10	19	28	0	6	5.2045	2.6376
11	17	44	0	11	7.1163	2.6114

Figure 6.28: Results of individual capillaries, measurements in pixels

Slope calculations

The results of all three different approaches for calculating the slope
of the capillaries are presented in the following matrices.

- Based on the slope of its bounding box

capillaryNo	bbSlope	Slope	length	deviation
1	1.68	1.64	62.13	0.14
2	1.58	1.53	22.52	0.25
3	2.29	2.2	32.2	0.42
4	2.19	2.11	40.82	0.33
5	2.01	1.91	95.97	0.13
6	1.15	1.2	65.55	0.58
7	1.76	1.68	46.27	0.1
8	2.05	1.96	16.01	0.18
9	1.57	1.66	34.13	0.12
10	1.96	1.88	29.9	0.1
11	1.71	1.8	35.9	0.02

Figure 6.29: Slope of capillaries based on their bounding boxes, in rad

- Based on the slope of the biggest diameter of its convex hull

cNo	Slope	length	deviation
1	1.6	108.04	0.13
2	1.26	29.41	0.47
3	2.37	68.59	0.64
4	2.01	65.31	0.29
5	1.85	118.68	0.13
6	1.23	75.27	0.49
7	1.79	56.29	0.06
8	1.79	27.66	0.06
9	1.43	43.42	0.29
10	1.86	55.36	0.14
11	1.78	38.83	0.05

Figure 6.30: Slope of capillaries based on their convex hull, in rad

- Based on the slopes of the pixels of the skeleton

No	mainSlope30	deviation30	mainSlope45	deviation45
1	1.85	0.32	2.05	0.06
2	1.95	0.22	2.05	0.06
3	1.95	0.22	1.95	0.16
4	1.95	0.22	1.95	0.16
5	2.05	0.12	2.05	0.06
6	2.05	0.12	2.05	0.06
7	2.05	0.12	2.05	0.06
8	2.75	0.58	2.05	0.06
9	1.9	0.27	2.4	0.29
10	2.75	0.58	2.65	0.54
11	0.5	1.67	3.1	0.99

Figure 6.31: Slope of capillaries based on the pixels of the skeleton, in rad

The above results were based on the following histograms formed for every capillary.
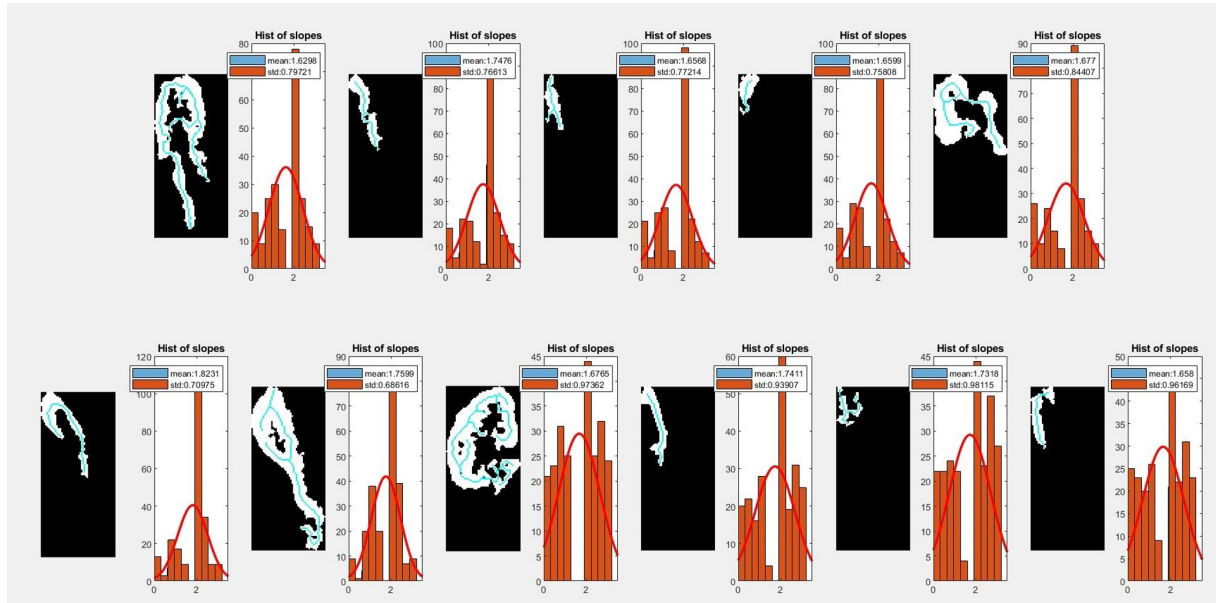
Figure 6.32: Histograms of slopes of skeleton pixels

6.3.2 Results comparison

A comparison on the results from the different approaches follows

- Slope Calculation

No	Slope30	Slope45	Bounding Box Slope	Convex Hull Slope
1	1.85	2.05	1.64	1.6
2	1.95	2.05	1.53	1.26
3	1.95	1.95	2.2	2.37
4	1.95	1.95	2.11	2.01
5	2.05	2.05	1.91	1.85
6	2.05	2.05	1.2	1.23
7	2.05	2.05	1.68	1.79
8	2.75	2.05	1.96	1.79
9	1.9	2.4	1.66	1.43
10	2.75	2.65	1.88	1.86
11	0.5	3.1	1.8	1.78

- Standard Deviation

No	Slope30	Slope45	Bounding Box Slope	Convex Hull Slope
1	0.32	0.06	0.14	0.13
2	0.22	0.06	0.25	0.47
3	0.22	0.16	0.42	0.64
4	0.22	0.16	0.33	0.29
5	0.12	0.06	0.13	0.13
6	0.12	0.06	0.58	0.49
7	0.12	0.06	0.1	0.06
8	0.58	0.06	0.18	0.06
9	0.27	0.29	0.12	0.29
10	0.58	0.54	0.1	0.14
11	1.67	0.99	0.02	0.05

6.3.3 Total Image Results

For the image as a total, the features calculated were the following:

Total image results

totalCapillaries	Density	Thickness
11	0.28114	0.52512

Figure 6.33: Total measures of the image, in pixels

Mean Capillary Results

m_width	m_height	m_mthick	std_thick
30.545	60.636	9.5528	5.6453

Figure 6.34: Total measures of mean capillary of the image, in pixels

Total width histogram from all capillaries

Hist_mean	Hist_std	Hist_median	Hist_25quartile	Hist_75quartile
11.307	8.3661	9	7.2245	13.702

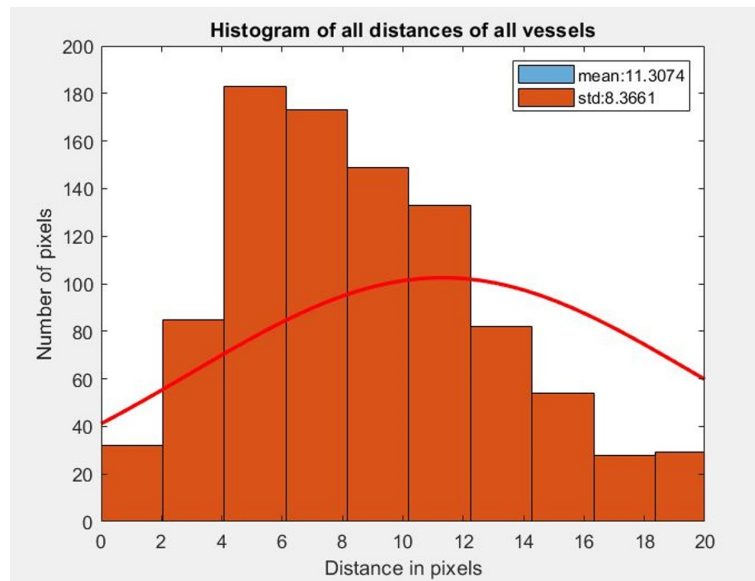Figure 6.35: Total measures of histogram of the image, in pixels

Figure 6.36: Width histogram from all capillaries, in pixels

6.3.4 Total slope and total deviation

Finally, the total slope and the total deviation for the capillaries in the image are calculated:

- Based on the slope of its bounding box

totalSlope	totalDeviation
1.78	0.22

Figure 6.37: Total slope and total deviation based on the slope of its bounding box, in rad

- Based on the slope of the biggest diameter of its convex hull

totalSlope	totalDeviation
1.72	0.25

Figure 6.38: Total slope and total deviation based on the biggest diameter of its convex hull, in rad

- Based on the slopes of the pixels of the skeleton

totalSlope30	totalDeviation30	totalSlope45	totalDeviation45
2.17	0.31	2.11	0.12

Figure 6.39: Total slope and total deviation based on the slopes of the pixels of the skeleton, in rad

Chapter 7

Discussion, Conclusion and Future Work

This final chapter of the thesis includes some final conclusions that are drawn after developing and testing the proposed method. As the present thesis provides a solid foundation for future work we have also included a section with recommendations for further research.

7.1 Conclusion

This work was focused on developing an automated system that could analyse the capillaries located in the nailfold area. The end goal for this particular system is to be used in the diagnostic process by physicians in order to evaluate a person's state of health. The system is able to pre-process the images, segment them and finally perform a series of measurements. After developing and testing the proposal, some of the main conclusions that can be drawn are that the system can successfully measure commonly used for the evaluation of the capillaries features and has also introduced a new set of elements that can be calculated on a capillaroscopic image. Thus, it has the potential to take into consideration a general estimate of the capillaroscopic image as well as focus on capillaries individually. As a result it can potentially substitute the tedious and prone to errors process of measuring manually these features and can also reduce the evaluation time required by the physicians.

7.2 Future Work

As the present thesis sets the foundations for a fully automated system that can classify the capillaries of a capillaroscopic image, future work concerns deeper analysis, testing and new approaches on the subject. Bellow follow a list of proposals on future work that can help expand and strengthen our results.

(i) *Testing on a larger dataset:* We believe that the system should be further tested using a larger dataset that would include images of capillaries of patients that have been diagnosed with different autoimmune diseases.

(ii) *Calculation of additional features:* Future research should certainly focus on extracting more features of the capillaries such as the width of the arterial and the venous limb, the intercapillary distance, the size of avascular areas and the presence of hemorrhages as the could play a critical role in the classification of a vessel.

(iii) *Classification:* Further work could examine the potential of using machine learning techniques for classifying the vessels based on the features calculated in the present thesis as well as other additional ones.

(iv) *Application development:* As the final goal of this thesis is to develop a fully automated system that can be used in the clinical practise it is important to build a user-friendly app that the physicians can easily install and use in their practise.

Abbreviations and acronyms

The next list describes several abbreviations and acronyms that were used within the body of the document

AARDA American Autoimmune Related Diseases Association

ACR American College of Rheumatology

ADWE Adaptive Damped Wave Equation

CDF Cumulative Distribution Function

CLAHE Contrast Limited Adaptive Histogram Equalization

DoB Difference of Boxes

DoG Difference of Gaussian

DWT Discrete Wavelet Transform

EULAR European League Against Rheumatism

LoG Laplacian of Gaussian

MCTD Mixed Connective Tissue Disease

NC   Nailfold Capillaroscopy

NML Non Local Means

SLE   Systemic Lupus Erythematous

SSc   Systemic Sclerosis

Bibliography

[1] E. Souza and C. Kayser, "Nailfold capillaroscopy: Relevance to the practice of rheumatology," *Revista Brasileira de Reumatologia (English Edition)*, vol. 44, 12 2014.

[2] S. Sangiorgi, A. Manelli, T. Congiu, A. Bini, G. Pilato, M. Reguzzoni, and M. Raspanti. (Journal of Anatomy, vol. 204, no. 2, pp. 123–131, 2004, ISSN: 0021-8782) Microvascularization of the human digit as studied by corrosion casting. [Online]. Available: https://www.ncbi.nlm.nih.gov/pmc/articles/PMC1571248/

[3] R. Usatine, J. L. Pfenninger, and D. L. Stulberg. (Elsevier Health Sciences, 2011, ISBN: 1437705804.) Dermatologic and cosmetic procedures in office practice.

[4] K. A. Tavakol ME, Fatemi A. (Biomed Res Int. 2015) Nailfold capillaroscopy in rheumatic diseases: Which parameters should be evaluated? [Online]. Available: https://www.ncbi.nlm.nih.gov/pmc/articles/PMC4569783/#B25

[5] C. K. Eduardo José do Rosário e Souza. (Rev. Bras. Reumatol. vol.55 no.3 São Paulo May/June 2015) Nailfold capillaroscopy: relevance to the practice of rheumatology. [Online]. Available: http://www.scielo.br/scielo.php?pid=S0482-50042015000300264&script=sci_arttext&tlng=en

[6] N. Drakos and R. Moore. Difference of gaussian (dog). [Online]. Available: http://fourier.eng.hmc.edu/e161/lectures/gradient/node9.html

[7] Wikipedia contributors, "Plagiarism — Wikipedia, the free encyclopedia," 2004, [Online; accessed 22-July-2004]. [Online]. Available: https://en.wikipedia.org/wiki/Adaptive_histogram_equalization

[8] A. Lerner, W. Patricia, and T. Matthias. (2015, 12) The world incidence and prevalence of autoimmune diseases is increasing.

[9] P. Doghramji. (2016) Screening and laboratory diagnosis of autoimmune diseases using antinuclear antibody immunofluorescence assayand specific autoantibody testing. [Online]. Available: https://www.aafp.org/dam/AAFP/documents/about_us/sponsored_resources/Quest_%20ANA-IFA_Monograph.pdf

[10] (2018) Quantitative evaluation of capillaroscopic microvascular changes in patients with established coronary heart disease. evaluación cuantitativa de los cambios microvasculares capilaroscópicos en pacientes con cardiopatía isquémica establecida. [Online]. Available: https://pubmed.ncbi.nlm.nih.gov/28870422/

[11] Wikipedia contributors, "Plagiarism — Wikipedia, the free encyclopedia," 2004, [Online; accessed 22-July-2004]. [Online]. Available: https://en.wikipedia.org/wiki/Capillary

[12] A. Shore. (Br J Clin Pharmacol. 200050(6):501-513) Capillaroscopy and the measurement of capillary pressure. [Online]. Available: https://www.ncbi.nlm.nih.gov/pmc/articles/PMC2015012/

[13] E. Maricq, HR LeRoy. (Arthritis Rheum 1973) Patterns of finger capillary abnormalities in connective tissue disease by 'wide-field'microscopy. [Online]. Available: https://www.ncbi.nlm.nih.gov/pubmed/4742842

[14] H. Groen, E. J. Borg, D. S. Postma, A. A. Wouda, T. WanderMark, and C. G. Kallenberg. (The American Journal of Medicine Volume 93, Issue 6, December 1992, Pages 619-627) Pulmonary function in systemic lupus erythematosus is related to distinct clinical, serologic, and nailfold capillary patterns. [Online].

Available: https://www.sciencedirect.com/science/article/abs/pii/000293439290194G

[15] N. Mugii, M. Hasegawa, T. Matsushita, Y. Hamaguchi, S. Horie, T. Yahata, and et al. (Rheumatology, Volume 50, Issue 6, June 2011, Pages 1091–1098,) Association between nail-fold capillary findings and disease activity in dermatomyositis. [Online]. Available: https://academic.oup.com/rheumatology/article/50/6/1091/1786170

[16] F. Granier, M. Vayssairat, P. Priollet, and E. Housset. (Arthritis Rheum. 1986;29(2):189–95.) Nailfold capillary microscopy in mixed connective tissue disease. comparison with systemic sclerosis and systemic lupus erythematosus. [Online]. Available: https://onlinelibrary.wiley.com/doi/abs/10.1002/art.1780290206

[17] K. Capobianco, R. Xavier, M. Bredemeier, V. Restelli, and J. Brenol. (Clin Exp Rheumatol. 2005;23(6):789–94) Nailfold capillaroscopic findings in primary sjögren's syndrome: clinical and serological correlations. [Online]. Available: https://www.clinexprheumatol.org/article.asp?a=2742

[18] L. Altomonte, A. Zoli, A. Galossi, L. Mirone, A. Tulli, F. Martone, P. Morini, P. Laraia, and M. Magarò. (Clin Exp Rheumatol. 1995;13(1):83–6.) Microvascular capillaroscopic abnormalities in rheumatoid arthritis patients. [Online]. Available: https://www.sciencedirect.com/science/article/abs/pii/S0026286212000556

[19] M. Candela, A. Pansoni, S. DeCarolis, G. Pomponio, A. Corvetta, A. Gabrielli, and G. Danieli. (Recenti Prog Med. 1998;89(9):444–9.) Nailfold capillary microscopy in patients with antiphospholipid syndrome. [Online]. Available: https://europepmc.org/article/med/9796374

[20] N. P. Doshi, G. Schaefer, and A. Merla. (2012 IEEE International Conference on Systems, Man, and Cybernetics (SMC). doi:10.1109/icsmc.2012.6377935) An evaluation of

image enhancement techniques for capillary imaging. [Online]. Available: https://ieeexplore.ieee.org/document/6377935

[21] G. Hamar, G. Horvath, Z. Tarjan, and T. Virag. (11th Mediterranean Conference on Medical and Biomedical Engineering and Computing 2007, 2007, Volume 16) Markov chain based edge detection algorithm for evaluation of capillary microscopic images. [Online]. Available: https://link.springer.com/chapter/10.1007/978-3-540-73044-6_212

[22] J. C. Riaño-Rojas, F. A. Prieto-Ortiz, L. J. Morantes, Sánchez-Camperos, E., and F. Jaramillo-Ayerbe. (2007 Sixth Mexican International Conference on Artificial Intelligence, Special Session (MICAI). doi:10.1109/micai.2007.40) Segmentation and extraction of morphologic features from capillary images. [Online]. Available: https://ieeexplore.ieee.org/document/4659305

[23] R. Nivedha, M. Brinda, K. V. Suma, and B. Rao. (2016 International Conference on Circuits, Controls, Communications and Computing (I4C). doi:10.1109/cimca.2016.8053300) Classification of nailfold capillary images in patients with hypertension using non-linear svm. [Online]. Available: https://ieeexplore.ieee.org/document/8053300

[24] A. F. Frangi, W. J. Niessen, K. L. Vincken, and M. A. Viergever. (Med. Image Comput. Comput. Assist. Interv., 2000) Multiscale vessel enhancement filtering. [Online]. Available: https://www.researchgate.net/publication/2388170_Multiscale_Vessel_Enhancement_Filtering/citation/download

[25] L. Shijian, L. Jiang, H. L. Joo, Z. Zhuo, N. M. Tan, K. W. Wing, L. Huiqi, and T. Y. Wong. (2009 Annual International Conference of the IEEE Engineering in Medicine and Biology Society. doi:10.1109/iembs.2009.5332917,) Automatic fundus image classification for computer-aided diagonsis.

[26] K. Zuiderveld. (chapter Contrast Limited Adaptive Histogram Equalization, pp. 474–485. Academic Press Professional, Inc., San Diego, CA, USA, 1994.) Graphics gems iv. [Online].

Available: http://cas.xav.free.fr/Graphics%20Gems%204%20-%20Paul%20S.%20Heckbert.pdf

[27] K. Koonsanit, S. Thongvigitmanee, N. Pongnapang, and P. Thajchayapong. (2017 10th Biomedical Engineering International Conference (BMEiCON). doi:10.1109/bmeicon.2017.8229130) Image enhancement on digital x-ray images using n-clahe. [Online]. Available: https://ieeexplore.ieee.org/document/8229130

[28] Wikipedia contributors, "Plagiarism — Wikipedia, the free encyclopedia," 2004, [Online; accessed 22-July-2004]. [Online]. Available: https://en.wikipedia.org/wiki/Otsu%27s_method

[29] N. P. Doshi, G. Schaefer, and S. Y. Zhu. (2013 IEEE International Conference on Systems, Man, and Cybernetics. doi:10.1109/smc.2013.438) An improved binarisation algorithm for nailfold capillary skeleton extraction. [Online]. Available: https://ieeexplore.ieee.org/document/6722191

[30] L. Lo, J. Y. Chiang, and Y. Cai. (2011 IEEE 11th International Conference on Bioinformatics and Bioengineering. doi:10.1109/bibe.2011.14) Three-dimensional vision-based nail-fold morphological and hemodynamic analysis. [Online]. Available: https://ieeexplore.ieee.org/document/6089806/